Mullard Technical Communications

JANUARY 1974
Volume 13 Number 121

Contents

2 Cleaning processes for Mullard resistors and capacitors on printed-wiring boards

15 Deflection system design for 110° shadowmask tubes

31 Phase II horizontal deflection circuit and its design principles

Mullard Limited Mullard House Torrington Place London WC1E 7HD

Mullard Technical Communications

VOLUME 13 NUMBER 121 January 1974

Cleaning processes for Mullard resistors and capacitors on printed-wiring boards *K. W. Stanley and M. H. Dryden* 2

Deflection system design for 110° shadowmask tubes *J. Kaashoek* 15

Phase II horizontal deflection circuit and its design principles 31

This journal records developments in the application of electronics in science, industry, and the home. It contains information on the properties and performance of solid-state devices, valves and tubes, and associated components and assemblies. The practical circuits given are designed to provide the best working conditions and performance for the devices used. The design principles may be used (so far as device ratings allow) for adaptation to meet particular requirements. Current data should be consulted before any circuit is considered for production. Mullard Limited can normally supply only those devices or assemblies listed in the Company's current catalogues. Availability in quantity should be confirmed.

All information is published in good faith, but because of the wide variety of situations in which this information may be used, we cannot accept any responsibility for loss or damage resulting from unsatisfactory performance. Publication of this information does not imply any authority or licence for the utilisation of any patented feature.

Four issues are published each year and issued free of charge to equipment designers, research organisations, laboratories, libraries, educational establishments, and consultants. Requests for addition to the mailing list must be made on the official stationery of the establishment concerned.

Technical enquiries should be addressed to the Editor. Abstracts or references should mention both source and authors. Requests for republication or translation should be made to the Editor in writing.

'Mullard' is the trade mark of Mullard Limited and is registered in most of the principal countries of the world.

Editor: E. G. Evans Assistant Editor: M. J. Prescott
Central Technical Services, Mullard Limited, New Road, Mitcham,
Surrey, CR4 4XY. Telephone: 01-648 3471. Telex 22194

Mullard Limited, Mullard House, Torrington Place, London, WC1E 7HD
Telephone: 01-580 6633 Telex: 264341

©Mullard Limited, 1974

Made and Printed in England by
WIGHTMAN AND COMPANY LIMITED, 1/3 BRIXTON ROAD, LONDON SW9 6DS

Cleaning processes for Mullard resistors and capacitors on printed-wiring boards

K. W. Stanley and M. H. Dryden
Mullard Limited

UDC 621.3.049[621.316.8][621.319.4]
UDC 621.798.8[66.062][536.423][534-8]
UDC 621.791.04

Post-assembly cleaning of printed-wiring boards carrying Mullard resistors and capacitors, to remove residues of soldering flux, is examined in depth. The results of tests carried out to determine component compatibility with various cleaning processes are presented and discussed.

INTRODUCTION

The subject of this article is the compatibility of Mullard passive components, in particular resistors and capacitors, with the cleaning processes used for removing flux residues and other contaminants from printed-wiring boards after soldering. Although the problem of flux residue removal may at first sight be considered trivial, considerable research has been carried out by the manufacturers of cleaning equipment to ensure the availability of processes capable of cleaning to the highest standards.

The complete removal of contaminants from soldered boards is essential where Government and Military specifications are to be met, and is in all cases desirable. Recently many manufacturers have begun to clean all boards as a matter of routine; not all, however, have met with success. There are several ways in which the cleaning operation can fail to give satisfactory results.

It is possible that the process selected gives poor cleaning results, that is, incomplete removal of flux. Alternatively, flux may be efficiently removed but at too great a cost in terms of capital equipment, maintenance (solvent replacement, etc.), labour, or all three. It is obviously necessary to choose a cleaning process which is cost-effective.

A less obvious failing of certain cleaning processes, and of many available solvents, is that they cause damage to the boards and components being cleaned. Considered in isolation there are many solvents for flux residues, but the solvent must distinguish between the rosinous flux residues and the resin- or elastomer-based materials used in components and insulation.

In this article a number of cleaning processes are described and their compatibility with Mullard resistors and capacitors investigated. It is profitable initially to examine the process of soldering, which gives rise to the necessity for cleaning the boards.

SOLDERING

Soldering is the standard method of permanently connecting two or more conductors, with the use of heat and a solder alloy. The object is to establish metallic, and therefore electrical, continuity between the conductors by means of an unbroken film of solder: when this is obtained the solder is said to have wetted the joint.

Deposits of dirt, grease and oxide on metal surfaces will prevent wetting by molten solder, and must be removed. Cleaning before soldering, however, is insufficient because oxides will generally form on metal surfaces while the metals are being heated in air. This is overcome by applying flux to the joint.

The flux must remove the film of tarnish (oxides and sulphides) from the members to be joined, leaving a clean metallic surface to which solder can adhere. Then, to prevent oxidation during the soldering process, the flux covers the cleaned surfaces making it impossible for atmospheric oxygen to come into contact with them. Additionally the flux assists in heat transfer to the joint, and it also reduces the surface tension of the molten solder, so that the surfaces to be joined are wetted more quickly. The more quickly a soldered joint is made, the less is the likelihood of thermal damage to the components being soldered.

Soldering techniques

Few printed-wiring boards today are produced using the traditional hand method, whereby the members to be joined are heated by a hand-held iron, and solder is applied in the form of wire. In recent years mechanical methods of soldering have been devised, and these are more often used for production work. Soldering components to printed-wiring boards is economically performed by either of two mechanical methods: dip soldering and flowsoldering.

Dip soldering

In dip soldering, flux is applied to the board; it is then dipped to a predetermined level in a bath of molten solder Before dipping, the board is at room temperature. It is raised to solder temperature by thermal conduction from the molten solder mass, which is maintained at a suitable temperature by a thermostatically-controlled heater. The surface of the molten solder quickly becomes contaminated with oxides, which prevent wetting, so baths are often fitted with wiper blades which sweep the surface before each dipping.

To assist in the displacement of flux from the joint by solder it is usual to lower the board on to the bath at a small angle. This allows gases, produced by evaporation of solvent from the flux, to escape more readily. Withdrawal of the board from the bath is preceded by tilting the board at a steeper angle. Excess solder then drains into the bath, and the risk of adjacent contacts becoming bridged with solder is reduced.

Flowsoldering

In flowsoldering (also known as wave soldering) the underside of the board, travelling on a conveyor over a special solder bath, cuts the crest of a molten solder wave, which is produced by an immersed pump forcing solder up through a slot. The solder wave is always free from contamination because it is pumped from below the surface of the solder reservoir. To improve solderability and promote good drainage of solder, tinning oils have been injected into the solder wave, but the presence of these oils can increase the cleaning problems encountered later.

The printed-wiring board passes in succession over a wave of flux, a pre-heating area and the solder wave as shown in Fig. 1. The flux wave operates in the same way as the solder wave, and the object of the pre-heater is partially to dry the flux. This removes by evaporation some of the solvent from the flux, bonding the flux to the board and preventing excess solvent from evaporating in the solder wave where it could cause blow-holes to appear in the joints. The pre-heating also prevents chilling of the solder wave, reducing the solder times, and it lessens the thermal shock to the components when the board is soldered. Typical pre-heating temperatures reached by the board range from 60 to 120°C: it will be shown later that the temperature of the board during pre-heating has considerable influence on the ease of removal of flux residues. The pre-heating temperature can be adjusted by varying the speed of the conveyor, and hence the length of time during which the board is above the heater. Alternatively, the power output of the heater itself, or the physical separation of the conveyor and the heater, may be varied.

Flux

As has been pointed out, the soldering flux has a multiple action: tarnish removal and the prevention of retarnishing; heat transfer to the joint; and assistance with wetting of the joint by the solder.

The removal of metal oxides from a metal surface can be accomplished by a number of different chemical processes. Those normally employed in soldering fluxes are:

Dissolution of the oxide, forming a salt and water;
Reduction of the oxide to the metal;
Electroless-plating.

The first reaction is the one employed for electrical purposes, and will be considered in detail below. Reducing fluxes are generally gaseous; they remove oxygen from metal oxides leaving a film of finely-divided metal powder. Electroless-plating fluxes (commonly called reaction fluxes) leave a thin film of metal on the surface, in much the same way as copper sulphate solution will leave a film of copper on iron or steel.

Fluxes used in the electronics industry convert metal oxides to a salt and water; they must therefore be acidic. The material used is rosin (colophony), a grade of natural abietic acid. This is dissolved in a vehicle, normally an organic solvent such as isopropanol, whose purpose is to permit the flux to be applied in liquid form. Unfortunately rosin used alone has a slow and mild action, which makes it difficult to achieve good, reproducible lead-solderability when components from a number of different sources are being used. For this reason it is customary to add to the flux a small proportion ($< 1\%$) of a more active chemical ('activator') to improve solderability by scavenging metal oxides.

The typical flux, then, consists of a mixture of rosin and activator, dissolved in an organic vehicle which quickly evaporates as the joint rises to soldering temperature. The activator may well be a hydrohalide salt of an aliphatic amine, for instance the hydrochloride $R.NH_3^+Cl^-$ where R represents an organic, aliphatic group. The mixture becomes more complicated as a result of the 'activity' of the mixture during the few seconds required for soldering, and the reaction mechanism can be summed up by the

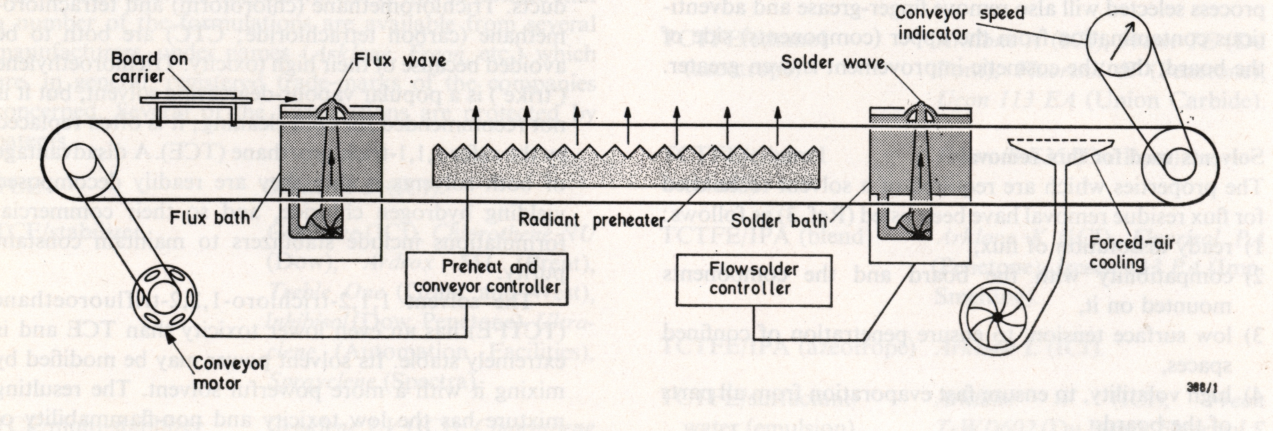

Fig. 1—Flowsolder process

following equations, using amine hydrochloride activator as an example (Ref. 1):

$$R.NH_3^+Cl^- \longrightarrow R.NH_2 + HCl$$
$$MO + 2HCl \longrightarrow MCl_2 + H_2O \quad (M = \text{metal})$$
$$R.NH_2 + HCl \longrightarrow R.NH_3^+Cl^-$$

This simplified model serves to show that flux residues which will be found on the printed-wiring board include, as well as rosin and activator, the metal halide which is the flux reaction product. Commercial fluxes may contain different activator systems, and so different residues will remain on the board after soldering. Each will pose its own removal problem. The colour photograph, Fig. 2 (which for ease of comparison with the other photographs appears on page 12), shows a board after soldering, with flux residues.

A recent development is flux incorporating an activator system which operates at the pre-heating temperature but is de-activated by the heat of the solder wave. The use of this flux is not, at present, widespread, but it is claimed that the flux residue is innocuous and need not be removed after soldering.

CLEANING

If pure rosin were used as soldering flux, then the residues found on printed-wiring boards after soldering would be (as is pointed out in Ref. 2) hard, non-corrosive, non-hygroscopic and non-conducting. The removal of these residues would be a less important, though still desirable, adjunct to the board assembly process. The presence in practical fluxes of an activator, however, necessitates post-assembly cleaning.

Cleaning boards after soldering is made necessary, firstly, by the corrosion risk associated with many flux activator systems. The possibility of this corrosion is least acceptable in assemblies with fine conductor patterns.

Cleaning the flux residues from the board permits a good bond with any conformal coating or potting compound which may subsequently be applied. Testing and inspection are facilitated when the board is clean, and the insulation resistance of the board surface is improved, particularly important where the spacing between conductors is small.

Lastly, but of increasing importance commercially, cleaning improves the assembly cosmetically. If the cleaning process selected will also remove finger-grease and adventitious contamination from the upper (components) side of the board, then the cosmetic improvement is even greater.

Solvents used for flux removal

The properties which are required of a solvent to be used for flux residue removal have been listed (Ref. 3) as follows:

1) ready dissolution of flux,
2) compatibility with the board and the components mounted on it,
3) low surface tension, to ensure penetration of confined spaces,
4) high volatility, to ensure fast evaporation from all parts of the board,
5) purity, to ensure that no residue is left on the board,
6) recoverability, for economy in use,
7) low flammability and low toxicity, for simplicity of handling,
8) good electrical properties, that is high resistivity.

Examination of the above list indicates that the requirements are most likely to be met by an organic solvent, which will have to be carefully chosen if the compatibility, flammability and toxicity requirements are to be satisfied.

Organic solvents

Organic solvents commonly used in industry can be divided into three major groups (Ref. 4).

1) Hydrocarbons. The group of hydrocarbon solvents comprises two sub-groups:
   a) Aliphatic hydrocarbons, such as petroleum spirit (petroleum ether), white spirit (mineral spirit), paraffin (kerosene);
   b) Aromatic hydrocarbons, such as benzene, toluene, xylene, solvent naphtha.

   These solvents are widely employed for oil and grease removal, and are not recommended by their suppliers for flux removal. Although they have low solvency for plastics, and may therefore be component-compatible, they are flammable and those in group (b) represent a health hazard.

2) Alcohols, Esters and Ketones. This group includes a wide range of industrial solvents, such as ethanol, isopropanol (IPA), ethyl acetate, methyl ethyl ketone (MEK), acetone.

   These are powerful solvents of low toxicity, but they are highly flammable and not recommended for production use. They remove flux efficiently, but will dissolve or soften many plastics used in component manufacture.

3) Halogenated solvents. These solvents, which are all non-flammable, are often recommended for flux removal. There are wide variations in solvency and other properties within this group, and it is important to choose the correct formulation.

   Dichloromethane (methylene chloride), a powerful solvent, is an ingredient of many paint-stripping products. Trichloromethane (chloroform) and tetrachloromethane (carbon tetrachloride; CTC) are both to be avoided because of their high toxicity. Trichloroethylene ('trike') is a popular vapour-degreasing solvent, but it is not recommended for cold cleaning; it is often replaced by the safer 1,1,1-trichloroethane (TCE). A disadvantage of both solvents is that they are readily decomposed yielding hydrogen chloride, and so their commercial formulations include stabilizers to maintain constant purity.

   The solvent 1,1,2-trichloro-1,2,2-trifluoroethane (TCTFE) has an even lower toxicity than TCE and is extremely stable. Its solvent power may be modified by mixing it with a more powerful solvent. The resulting mixture has the low toxicity and non-flammability of TCTFE, but a solvency characteristic similar to that of the added constituent, although slower-acting because of the dilution with TCTFE.

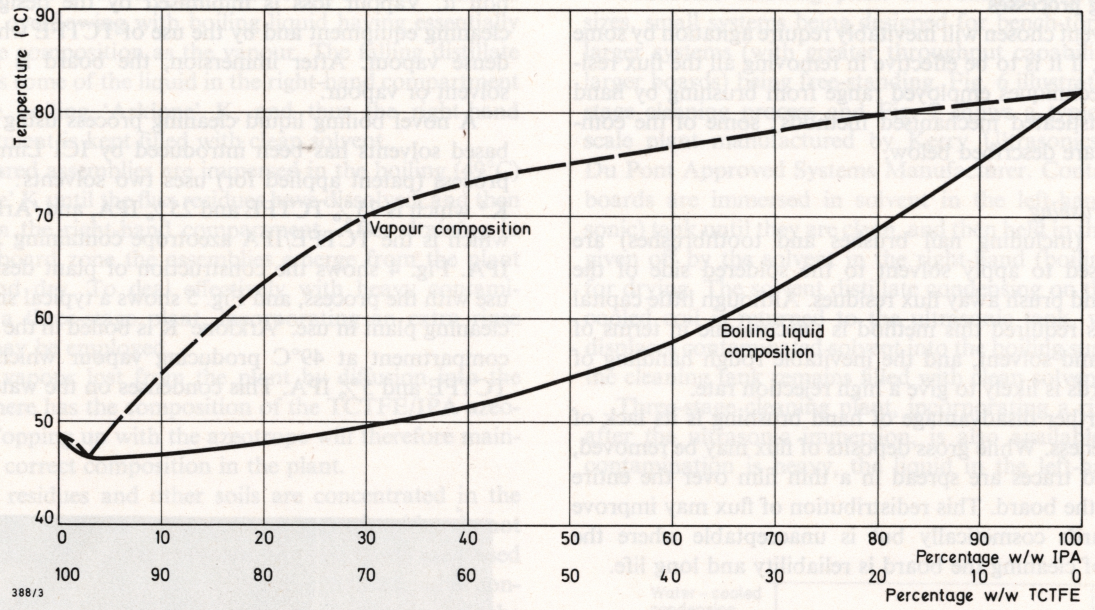

Fig. 3—Phase diagram for mixtures of 1,1,2-trichloro-1,2,2-trifluoroethylene (TCTFE) and isopropanol (IPA)

Such a mixture may be either a simple blend, or an azeotrope. An azeotrope is a mixture whose proportions are such that when the liquid boils the vapour generated contains the two substances in the same proportion as in the mother liquid. Continuous boiling will therefore not affect the composition of the liquid. For a mixture of, say, TCTFE and isopropanol (IPA) the azeotropic composition is 2·9% w/w IPA: this is the proportion indicated by the intersection of the liquid and vapour curves in Fig. 3 which is a phase diagram for mixtures of TCTFE and IPA.

Proprietary solvents

The list below includes most of the solvents available and recommended for flux removal, together with trade-names and the names of the manufacturers. It will be noticed that a number of the formulations are available from several manufacturers, under names (*Arklone*, *Freon*, etc.) which are, in general, registered trade-marks of the companies concerned. Several of the formulations are protected by patents.

TCE	*Genklene P* (ICI).
TCE/stabilizer	*Genklene* (ICI), *Chlorothene NU* (Dow), *Ardrox 551* (Brent), *Treble One* (Grant and West), *Inhibisol* (Dow, Penetone), *Ultraclene* (Automation Facilities), *Sprayclene* (Spectra).
TCE/multi-stabilizer	*Genklene LV* (ICI), *Chlorothene VG* (Dow).
TCE/perchloroethylene (blend)	*Genklene VA* (ICI), *Treble One Plus* (Grant and West).
TCTFE	*Arklone P* (ICI), *Freon TF* (Du Pont), *Fluorisol* (Penetone), *Isceon 113* (Imp. Smelting), *Flugéne 113* (Rhône-Progil), *Frigen 113 CR* (Hoechst), *Kaltron 113 MDR* (Kalichemie), *Edifren 113* (Montedison), *Ucon 113* (Union Carbide).
TCTFE/acetone (azeotrope)	*Arklone B* (ICI), *Freon TA* (Du Pont), *Isceon 113A* (Imp. Smelting).
TCTFE/dichloromethane (azeotrope)	*Arklone E* (ICI), *Freon TMC* (Du Pont), *Isceon 113C* (Imp. Smelting).
TCTFE/ethanol (azeotrope)	*Arklone A* (ICI), *Freon TE* (Du Pont), *Fluorisol E* (Penetone), *Ucon 113 EA* (Union Carbide).
TCTFE/ethanol (blend)	*Freon T-E35* (Du Pont).
TCTFE/IPA (blend)	*Arklone K* (ICI), *Fluorisol PA* (Penetone). *Isceon 113 PA* (Imp. Smelting).
TCTFE/IPA (azeotrope)	*Arklone L* (ICI).
TCTFE/surfactant/ water (emulsion)	*Arklone W* (ICI), *Freon T-WD602* (Du Pont), *Fluorisol S* (Penetone).

Cleaning processes

The solvent chosen will inevitably require agitation by some method, if it is to be effective in removing all the flux residues. Techniques employed range from brushing by hand to sophisticated mechanised methods: some of the commonest are described below.

Hand brushing

Brushes (including nail brushes and toothbrushes) are often used to apply solvent to the soldered side of the board and brush away flux residues. Although little capital outlay is required this method is uneconomic in terms of labour and solvent, and the inevitable rough handling of the boards is likely to give a high rejection rate.

A further disadvantage of hand brushing is its lack of effectiveness. While gross deposits of flux may be removed, dissolved traces are spread in a thin film over the entire area of the board. This redistribution of flux may improve the boards cosmetically but is unacceptable where the object of cleaning the board is reliability and long life.

Kiss-cleaning

Kiss-cleaning the board is a markedly more effective method of cleaning than hand brushing. The fluxed side of the board is brought into contact with the surface of the cleaning solvent which is contained in a static bath. The solvent may be ultrasonically agitated, or the bath may contain rotary brushes, flush with the surface, to give a scrubbing action. Contamination of the solvent can be kept to a minimum if it is continually redistilled in a still connected to the bath.

A disadvantage of both the above methods is that the top surface (components side) of the board is not cleaned. Residues of finger grease, and of flux which has passed through holes in the board by capillary action, are not removed. Furthermore the throughput of boards is low. For complete cleaning of both sides of the board, total immersion of the board is indicated. If this method is used it is clearly necessary to make a very careful choice of solvent, to ensure compatibility with the components.

Boiling liquid processes

A simple, effective and inexpensive method of agitating a solvent in which boards are immersed for cleaning is to boil it. Vapour loss is minimised by the design of the cleaning equipment and by the use of TCTFE which has a dense vapour. After immersion, the board is rinsed in solvent or vapour.

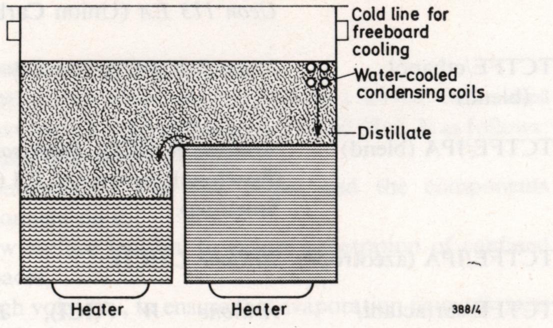
Cold line for freeboard cooling
Water-cooled condensing coils
Distillate
Heater
Heater
388/4

Fig. 4—Two-stage plant for use with the ICI flux-removal process

A novel boiling liquid cleaning process using TCTFE-based solvents has been introduced by ICI Limited. The process (patent applied for) uses two solvents: 'Arklone' K* which is 75% TCTFE and 25% IPA, and 'Arklone' L* which is the TCTFE/IPA azeotrope containing 2·9%w/w IPA. Fig. 4 shows the construction of plant designed for use with the process, and Fig. 5 shows a typical small-scale cleaning plant in use. 'Arklone' K is boiled in the left-hand compartment at 49°C producing vapour which is 95% TCTFE and 5% IPA. This condenses on the water-cooled coil and falls into the right-hand compartment which is filled to overflowing with boiling liquid having essentially the same composition as the vapour. The falling distillate displaces some of the liquid in the right-hand compartment into the boiling 'Arklone' K, and thus the right-hand compartment is kept filled with clean solvent.

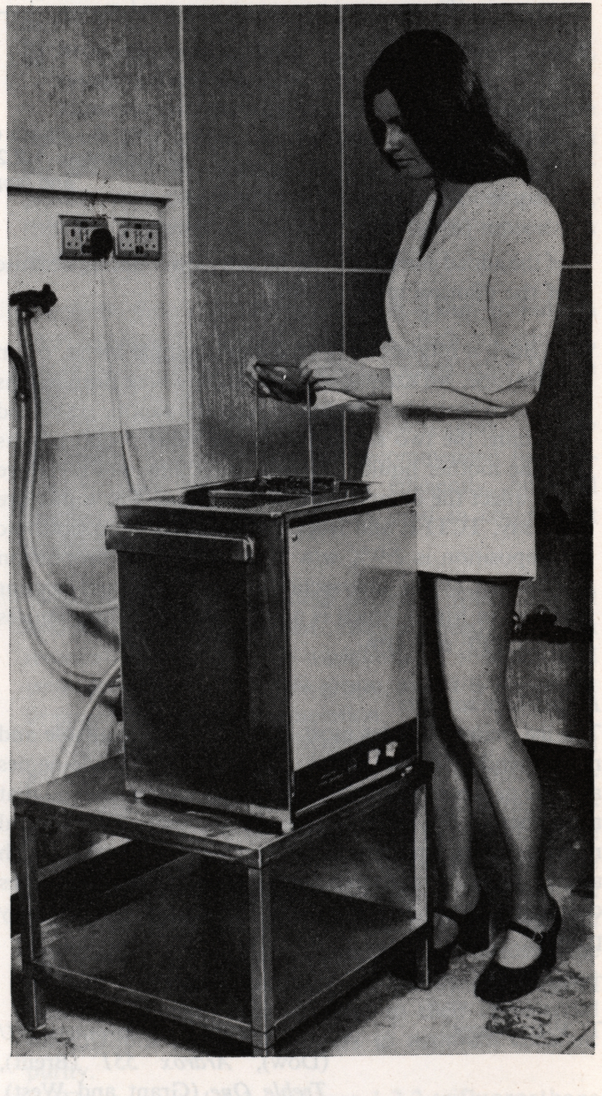

Fig. 5—Typical small-scale plant for use with the ICI flux-removal process, in use
(Photograph by courtesy of ICI Limited)

Soldered assemblies are immersed in the boiling (49°C) 'Arklone' K until the flux residues have dissolved, and then rinsed in the right-hand compartment. After draining in the freeboard zone the assemblies emerge from the plant clean and dry. To deal effectively with heavy contamination, a three-stage plant, incorporating an extra rinse stage, may be employed.

Any vapour lost from the plant by diffusion into the atmosphere has the composition of the TCTFE/IPA azeotrope. Topping up with the azeotrope will therefore maintain the correct composition in the plant.

Flux residues and other soils are concentrated in the left-hand wash tank. Low concentrations of residue do not affect the cleaning effectiveness since the boards are rinsed in clean solvent after washing. When the flux residue contamination reaches 5 to 7%w/w flux in 'Arklone' K the solvent must be replaced. It is possible to redistill the contaminated solvent using the cleaning plant itself as a still, but for a small plant such as that shown in Fig. 5 this is unlikely to be economic.

Ultrasonic cleaning

The solvent agitation required for effective cleaning may also be achieved by ultrasonic irradiation. Electrical oscillations at frequencies above the upper limit of audibility are generated, amplified, and applied to a transducer which is bonded to one wall of the solvent bath. The mechanical oscillations of the transducer are propagated as pressure waves through the solvent, reaching every part of the bath and the printed-wiring boards immersed in it.

To ensure that the irradiation is thorough in its action, it is recognised that the wavelength of the ultrasound should be of the order of the smallest dimension of any cavity which must be penetrated. For this reason the ultrasonic frequency must be chosen (knowing the speed of sound in the solvent to be used) for individual applications. For cleaning printed-wiring boards with TCTFE-based solvents, frequencies in the range 25 to 50kHz have generally been employed.

To remove effectively such soils as highly-activated fluxes it is necessary to induce the phenomenon known as cavitation. Cavitation—the formation of vapour bubbles within the solvent—occurs when, at high irradiating power, the (negative) pressure amplitude of the agitation exceeds the solvent hydrostatic pressure. The bubbles necessarily collapse when this pressure defect returns to zero, and in so doing release large quantities of energy. Since cavitation occurs preferentially at nuclei such as surface irregularities in the workpiece, the cavitation energy is released where it is most needed, and the cleaning effectiveness is greatly improved. The majority of ultrasonic cleaners for use with printed-wiring boards use frequencies of the order of 40kHz and acoustic intensities above the cavitation threshold, but a lower frequency (say 25kHz) with intense cavitation may in certain circumstances be more desirable.

Ultrasonic cleaning plant is available in a range of sizes, small systems being designed for bench-top use and larger systems (with greater throughput capability or for larger boards) being free-standing. Fig. 6 illustrates a two-stage cleaning process and Fig. 7 shows a typical small-scale plant manufactured by Kerry Ultrasonics Ltd., a Du Pont Approved Systems Manufacturer. Contaminated boards are immersed in solvent in the left-hand (ultrasonic) tank until they are clean, and then held in the vapour given off by the solvent in the right-hand (boiling) sump for drying. The solvent distillate condensing on the water-cooled coil is returned to the ultrasonic tank, whence it displaces contaminated solvent into the boiling sump. Thus the cleaning tank remains filled with clean solvent.

Three-stage cleaning plant, incorporating a rinse stage after the ultrasonic immersion, is also available. Where contamination is heavy, the liquid in the left-hand tank

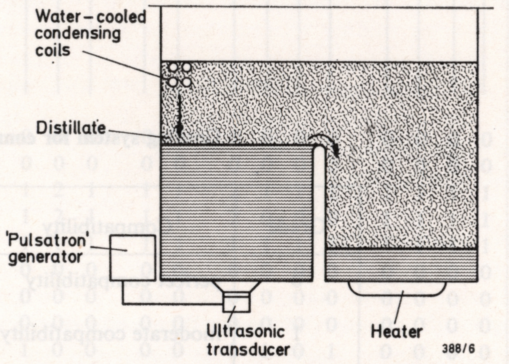

Fig. 6—Two-stage ultrasonic cleaning plant

Fig. 7—Typical small-scale two-stage ultrasonic cleaning plant. Bench-mounted overall dimensions: 31·7in (length) × 11·8in (width) × 24·4in (height)
(Photograph by courtesy of Kerry Ultrasonics Ltd.)

---

*B.P. 1 026 603

may be continuously passed through enclosed multiple-loop filters to remove particulate contamination. A further facility is refrigeration, rather than water-cooling, for the solvent reflux coils and for the ultrasonic cleaning liquid (which can thus be maintained at its optimum temperature).

Before installing cleaning plant of any description the user should ensure that the system chosen is appropriate to his application. Equipment manufacturers and solvent suppliers are normally anxious to ascertain that the process selected is capable of effective cleaning, and that it will not damage the components to be cleaned.

COMPONENT COMPATIBILITY

The two most important factors to be considered when assessing the effectiveness of a solvent or a process used for cleaning printed-wiring boards are its flux-removing ability and its compatibility with the boards to be cleaned, particularly with the components mounted on the boards.

With the co-operation of Du Pont de Nemours International S.A. (Freon and Valclene Products Dept.) and ICI Limited (Mond Division), tests were carried out on Mullard resistors and capacitors using a number of different solvents and cleaning processes. The tests are described and the results discussed below; component compatibility and flux removal are dealt with separately.

Numerous Mullard resistors and capacitors were cleaned by a variety of processes. After cleaning, each component was visually examined for evidence of damage, such as discolouration, damage to the coating or encapsulation, removal or obliteration of the marking.

Any damage to the component was assessed according to the grading system shown in Table 1. It will be understood that the particular nature of the damage suffered by a component must depend upon the construction of the component.

The tests carried out by ICI used processes based on TCTFE (the ICI 'Arklone' range of solvents: see Table 2). In general the processes included immersion in either boiling or ultrasonically-irradiated solvent, followed by after-treatment either in another solvent or in solvent vapour.

TABLE 1

Grading system for compatibility of components with solvents

Grade	Compatibility	Component damage
0	perfect compatibility	Component unaffected
1	moderate compatibility	Component slightly affected: discolouration; efflorescence of wax coating; partial disappearance of marking
2	incompatibility	Component significantly affected: serious discolouration; blistering, cracking or pitting of lacquer; serious dissolution of encapsulation material; total disappearance or illegibility of marking.

TABLE 2

Composition of ICI 'Arklone' solvents used in the tests

'Arklone' P	pure trichlorotrifluoroethane (TCTFE)
'Arklone' L	TCTFE 97·1%, isopropanol 2·9% w/w (azeotrope)
('Arklone' L+	TCTFE 94·5%, isopropanol 5·5% w/w)
'Arklone' K	TCTFE 75%, isopropanol 25% w/w
'Arklone' A	TCTFE 95·5%, ethanol 4·5% w/w (azeotrope)
'Arklone' E	TCTFE 50·5%, dichloromethane 49·5% w/w (azeotrope)

Note: 'Arklone' L+ is the condensate obtained by distillation of boiling 'Arklone' K, and is not a commercially available product.

TABLE 3

Cleaning process used on each component, and grades of compatibility found

ICI cleaning processes

(Figures in parentheses indicate the duration of each stage, in minutes)

Mullard components tested	Boiling 'Arklone' E (5), 'Arklone' E vapour (¼)	Boiling 'Arklone' E (1), 'Arklone' E vapour (¼)	Ultrasonic 'Arklone' A (5), 'Arklone' A vapour (¼)	Ultrasonic 'Arklone' A (1), 'Arklone' A vapour (¼)	Boiling 'Arklone' A (5), 'Arklone' A vapour (¼)	Boiling 'Arklone' A (1), 'Arklone' A vapour (¼)	Boiling 'Arklone' K (5), Boiling 'Arklone' L+(½)	Boiling 'Arklone' K (1), Boiling 'Arklone' L+(¼)	Ultrasonic 'Arklone' L (5), 'Arklone' L vapour (¼)	Ultrasonic 'Arklone' L (1), 'Arklone' L vapour (¼)	Boiling 'Arklone' L (5), 'Arklone' L vapour (¼)	Boiling 'Arklone' L (1), 'Arklone' L vapour (¼)	Ultrasonic 'Arklone' P (5), 'Arklone' P vapour (1)	Ultrasonic 'Arklone' P (1), 'Arklone' P vapour (¼)	Boiling 'Arklone' P (5), 'Arklone' P vapour (¼)	Boiling 'Arklone' P (1), 'Arklone' P vapour (¼)
Carbon film resistors CR16/25/37 series	0	0	0	0	0	0	0	0	0	0	0	0	0	0	0	0
Metal film resistors MR25/30 series	0	0	0	0	0	0	0	0	0	0	0	0	0	0	0	0
Power metal film resistors PR37/52 series	2	2	1	1	2	1	1	1	2	1	1	1	1	1	1	1
Voltage dependent resistors E298 series	2	1	1	1	2	1	1	1	2	0	0	0	1	1	1	1
Voltage dependent resistors E299 series	1	1	1	1	1	1	1	1	1	1	1	1	1	1	1	1
PTC resistors VA8650	2	2	0	0	0	0	0	0	0	0	0	0	0	0	0	0
NTC resistors VA1000 series	2	0	0	0	0	0	0	0	0	0	0	0	0	0	0	0
Metallised film capacitors (moulded) 344 series	0	0	0	0	0	0	0	0	0	0	0	0	0	0	0	0
Metallised film capacitors (moulded) C281 series	1	1	1	1	0	0	0	0	1	1	0	1	0	0	0	0
Metallised film capacitors (lacquered) C280 series	2	2	1	1	2	1	2	1	1	1	2	1	2	1	1	1
Film/foil capacitors C296 and 347 series	0	0	0	0	0	0	0	0	0	0	0	0	0	0	0	0
Ceramic plate capacitors C333 series	0	0	0	0	0	0	0	0	0	0	0	0	0	0	0	0
Polystyrene capacitors (sleeved) 424 series	1	1	1	1	1	1	1	1	1	1	1	1	1	1	1	1
Polystyrene capacitors (moulded) C295 series	2	2	1	1	1	1	1	0	2	1	1	0	1	1	1	1
Solid aluminium capacitors 121 series	1	1	1	1	1	1	1	1	1	1	1	1	1	1	1	1
Electrolytic capacitors 015/016/017 series	2	2	0	0	0	0	0	0	0	0	0	0	0	0	0	0

All the ultrasonic treatments were carried out at 40kHz with an intensity of 13W/litre at room temperature. The results of the tests are given in Table 3.

Analysis of the results of Table 3 (ICI tests) shows that many components were unaffected in any way by any of the solvents. Some, however, were particularly vulnerable and the damage suffered by these is detailed in Table 4.

The ICI flux-removal process using 'Arklone' K can be seen from Table 3 to be one of the least damaging to components. After 1 minute in the boiling solvent followed by a rinse, a total of only 6 components suffered minor (grade 1) damage: the lowest score obtained in this test. A similar process using 'Arklone' L gave equal compatibility but less effective cleaning—see Table 9. Cleaning with 'Arklone' E, the azeotropic mixture of TCTFE and dichloromethane, caused the most damage to components.

TABLE 4

Details of component damage ('Arklone' solvents)

Component	Nature of damage*
PR37/52 series	blistered lacquer
E298 series	blistered lacquer
E299 series	efflorescence of the wax impregnant
VA8650	blistered lacquer
VA1000 series	blistered lacquer
C281 series	reduced marking legibility
C280 series	blistered or cracked colour-coding lacquer
424 series	partly dissolved body
C295 series	dissolution of encapsulation
121 series	partial removal of red colour code
015/016/017 series	sleeve material cracked

*No electrical tests were carried out on these components.

Similar tests were carried out by Du Pont de Nemours International S.A. using their 'Freon' range of TCTFE-based solvents, detailed in Table 5. The processes tested included immersion in both boiling and ultrasonic solvent. Table 6 shows the processes and components tested, with the results in grades of compatiblity according to the scheme of Table 1.

Again, analysis of the results shows that many components are unaffected by cleaning. Where damage occurred it was, as shown in Table 7, similar to that found previously in the tests carried out with other proprietary solvents. Boiling and ultrasonic treatment in 'Freon' TE and 'Freon' TF both produced the minimum damage; 'Freon' TMC was the least compatible solvent.

From these two series of tests, it is evident that several solvents and cleaning processes have minimal (if any) visual effect on the components tested. Visual appearance, however, is but one criterion for the assessment of component compatibility; it is more important that the component electrical parameters remain unaltered.

TABLE 7

Details of component damage ('Freon' solvents)

Component	Nature of damage*
PR37/52 series	blistered lacquer
E298 series	blistered lacquer
E299 series	efflorescence of wax impregnant
VA8650	blistered lacquer
C280 series	blistered or cracked colour-coding lacquer
424 series	'crazing' effect on the film
C295 series	partial removal of encapsulant
015/016/017 series	sleeve material cracked

*No electrical tests were carried out on these components.

TABLE 5

Composition of Du Pont 'Freon' solvents used in the tests

'Freon' TF	pure trichlorotrifluoroethane (TCTFE)
'Freon' TE	TCTFE 95·5%, ethanol 4·5% w/w (azeotrope)
'Freon' TMC	TCTFE 50·5%, dichloromethane 49·5% w/w (azeotrope)

TABLE 6

Cleaning process used on each component, and grades of compatibility found

Du Pont solvent immersion processes*
(Figures in parentheses indicate the duration of each stage, in minutes)

Mullard components tested	Boiling 'Freon' TMC (3), Ultrasonic 'Freon' TMC (1)	Boiling 'Freon' TMC (1), Ultrasonic 'Freon' TMC (½)	Boiling 'Freon' TE (3), Ultrasonic 'Freon' TE (1)	Boiling 'Freon' TE (1), Ultrasonic 'Freon' TE (½)	Boiling 'Freon' TF (3), Ultrasonic 'Freon' TF (1)	Boiling 'Freon' TF (1), Ultrasonic 'Freon' TF (½)
Carbon film resistors CR16/25/37 series	0	0	0	0	0	0
Metal film resistors MR25/30 series	0	0	0	0	0	0
Power metal film resistors PR37/52 series	2	2	2	2	2	1
Voltage dependent resistors E298 series	2	2	0	0	0	0
Voltage dependent resistors E299 series	1	1	1	1	1	1
PTC resistors VA8650	2	2	0	0	0	0
NTC resistors VA1000 series	0	0	0	0	0	0
Metallised film capacitors (moulded) 344 series	0	0	0	0	0	0
Metallised film capacitors (moulded) C281 series	0	0	0	0	0	0
Metallised film capacitors (lacquered) C280 series	2	2	1	1	1	1
Film/foil capacitors C296 and 347 series	2	0	0	0	0	0
Ceramic plate capacitors C333 series	0	0	0	0	0	0
Polystyrene capacitors (sleeved) 424 series	2	2	0	0	0	0
Polystyrene capacitors (moulded) C295 series	2	2	2	2	2	2
Solid aluminium capacitors 121 series	0	0	0	0	0	0
Electrolytic capacitors 015/016/017 series	2	2	0	0	0	0

*Some of these are established cleaning processes.

Further components were subjected to the ICI flux removal process described on page 6. The cleaning programme, representing a worst-case condition, comprised immersion in boiling 'Arklone' K for 5 minutes followed by rinsing for 30 seconds in 'Arklone' L+.

The actual measurements made depend on the component studied. In general, the basic parameters of the component were checked against its specification, first immediately after cleaning and again after exposure to such environmental conditions as

BS2011: Part 2Ca: 1971 damp heat, steady state,	(IEC68-2 test C)
BS2011: Part 2Da: 1963 damp heat, cyclic,	(IEC68-2 test D)
BS2011: Part 2Na: 1967 rapid change of temperature, thermal shock in air.	(IEC68-2 test Na)

Both before and after the environmental exposure, only visual damage was found. No change in electrical parameters was observed and the components met their specifications in all respects, their performance showing no difference from that of a control batch of uncleaned components.

FLUX REMOVAL

The prime purpose of any cleaning process is to remove flux residues and other contaminants from the printed-wiring board. Ideally it should achieve this without leaving any stains or residues on the board, or attacking the components. The latter question, for Mullard resistors and capacitors, has been considered above. This section attempts to examine the cleaning effectiveness of various processes.

A range of passive components was mounted on glass-epoxy printed-wiring boards. The boards were fluxed by hand using a typical flux whose composition was as follows:

Rosin (colophony)	38·5%w/w
Dimethylamine hydrochloride	0·8%w/w
Isopropanol	60·7%w/w

(Excessive flux was applied so that some was present on the components side of the boards.) The boards were soldered on a Hollis soldering machine using 60/40 tin/lead solder, after preheating for approximately 1½ minutes during which time the maximum temperature reached by the boards was approximately 100°C.

The boards were then cleaned (by ICI Limited) using solvents based on TCTFE, and inspected under ×10 magnification. The cleaning processes included immersion in either boiling or ultrasonically-irradiated solvent, followed by after-treatment in solvent or vapour. All ultrasonic treatments were carried out at 40kHz with an intensity of 13W/litre at room temperature. The assessment of cleanliness is subjective; standards cannot accurately be defined. The boards were assessed visually according to Table 8, but it must be remembered that considerable gradation exists within each grade.

Stains are generally white, greyish or brown. Deposits consist of powdery material, white or greyish-white, and are generally accompanied by an uneven white bloom. Residues are traces of incompletely removed flux. Generally of shiny appearance, they are found concentrated near or beneath flat-mounted components.

TABLE 8

Cleanliness grading system

Cleanliness indication		Appearance of board		
Grade	Description	Stains	Deposits	Residues
0	No contamination	None	None	None
1	Insignificant contamination	Some small stains, hardly visible, scattered on board	Small, concentrated on spots and beneath components	Traces, especially beneath components
2	Slight contamination	Localized slight stains: spotty appearance	Slight deposits on spots and on base material. Thin uneven white bloom	Small quantities, near or beneath components
3	Significant contamination	Significant stains on major part of board	Powdery deposits on major part of board. Uneven white bloom	Significant scattered residues
4	Widespread contamination	Widespread stains on almost the entire board	Concentrated gross powdery deposits. Thick uneven white bloom on entire board	Gross residues on entire board

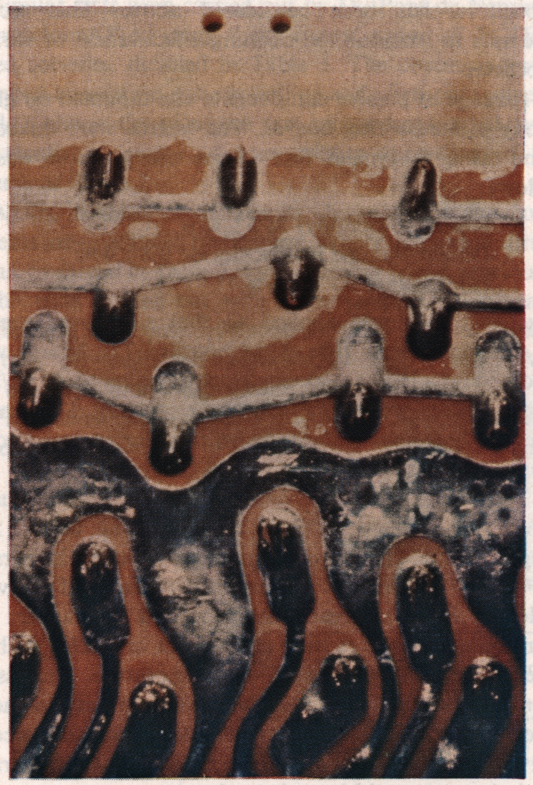

Fig. 2—Printed-wiring board after soldering, showing flux residues

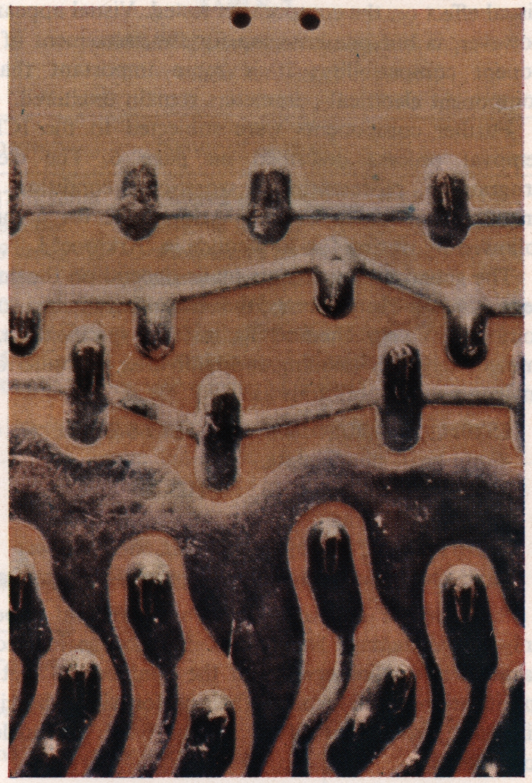

Fig. 8—Excessively pre-heated board, after cleaning, showing white stains

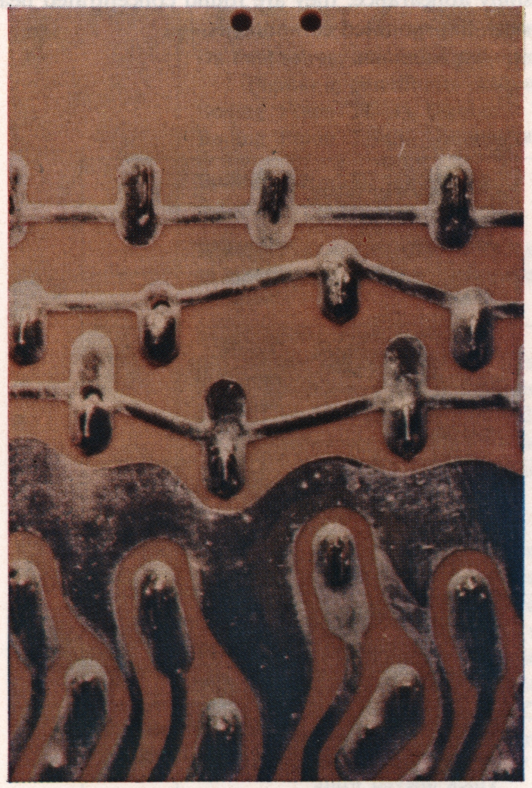

Fig. 9—Perfectly cleaned (grade 0) board

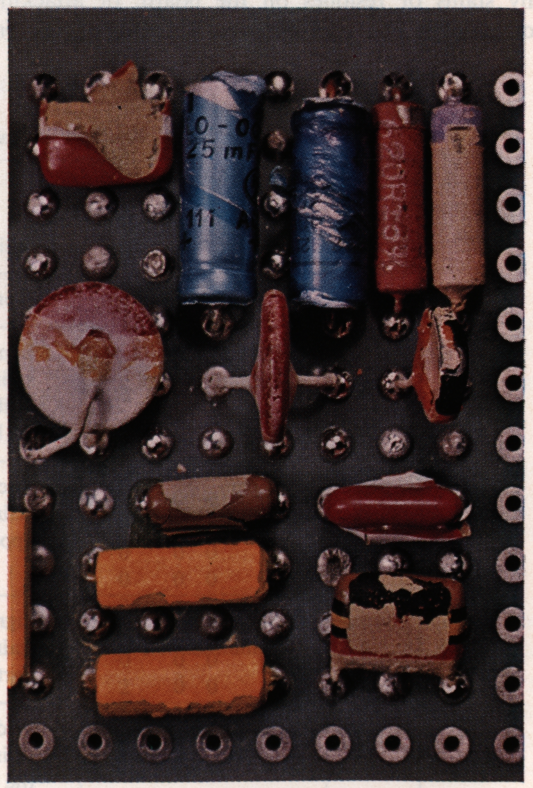

Fig. 10—Board after cleaning using a solvent containing dichloromethane, showing damaged components

TABLE 9

Cleanliness grades obtained by ICI cleaning processes

Storage time (h)	Cleaning process (figures in parentheses indicate duration of each stage, in minutes)	Cleanliness grade
190	Boiling 'Arklone' P (1), 'Arklone' P vapour (¼)	4
190	Boiling 'Arklone' P (5), 'Arklone' P vapour (¼)	4
190	Ultrasonic 'Arklone' P (1), 'Arklone' P vapour (¼)	4
190	Ultrasonic 'Arklone' P (5), 'Arklone' P vapour (¼)	4
50	Boiling 'Arklone' L (1), 'Arklone' L vapour (¼)	3
140	Boiling 'Arklone' L (5), 'Arklone' L vapour (¼)	3
140	Ultrasonic 'Arklone' L (1), 'Arklone' L vapour (¼)	2
140	Ultrasonic 'Arklone' L (5), 'Arklone' L vapour (¼)	3
50	Boiling 'Arklone' K (1), Boiling 'Arklone' L+(¼)	1
100	Boiling 'Arklone' K (5), boiling 'Arklone' L+(½)	2
140	Boiling 'Arklone' A (1), 'Arklone' A vapour (¼)	3
140	Boiling 'Arklone' A (5), 'Arklone' A vapour (¼)	3
140	Ultrasonic 'Arklone' A (1), 'Arklone' A vapour (¼)	3
140	Ultrasonic 'Arklone' A (5), 'Arklone' A vapour (¼)	3
550	Boiling 'Arklone' E (1), 'Arklone' E vapour (¼)	3
550	Boiling 'Arklone' E (5), 'Arklone' E vapour (¼)	3

The cleanliness of the printed-wiring boards obtained by various cleaning processes is shown in Table 9, and the results are discussed below.

Storage time

Under normal production conditions, it is to be expected that boards will be cleaned almost immediately after soldering. Certainly for direct comparison of the cleaning effectiveness of various solvents and processes it would have been desirable for the storage time to have been kept constant. For example, an increase in storage time from 50 hours to 100 hours for the boards cleaned in 'Arklone' K resulted in a decrease of cleanliness from grade 1 to 2 even though the cleaning time was increased by a factor of five. If this observation can be applied in reverse to some of the boards stored for a longer period, improved results may well be obtained at short storage times.

Pre-heating temperature

For the test described above, all the boards were pre-heated to 100°C before soldering. A second test was carried out to investigate the effect of varying the pre-heating temperature. Batches of boards were pre-heated to different temperatures in the range 65 to 125°C, before being flowsoldered. The variable pre-heating was accomplished by means of the calibration of the heater, and the temperature attained on the soldering side of the board was measured *in situ* on the conveyor, before the board reached the solder wave.

After soldering, the boards were aged for 4, 80 or 400 hours before cleaning. The cleanliness grades obtained in this test are shown in Table 10.

This test shows that with the boiling high-alcohol cleaning process considered, board cleanliness depends to a large extent on the pre-heating temperature. The contamination remaining on boards pre-heated to temperatures above 100°C consisted of white stains, the extent of which increased with temperature. These stains, which may be seen in Fig. 8, are thought to be insoluble residues of the flux activator. They were found not to affect the insulation resistance of the board. Ultrasonic cleaning systems and alternative fluxes were not investigated in relation to the parameters of Table 10.

TABLE 10

Variation of cleaning effectiveness with pre-heating temperature, storage time and immersion time

Pre-heating temperature (approx)	Storage time (h)	Immersion time in 'Arklone' K (minutes)	Cleanliness grade
65°C	4	½	0
	4	1	0
	80	½	0
	400	1	0
75 to 80°C	4	½	0
	4	1	0
	80	½	1
	400	1	1
85 to 95°C	4	½	0
	4	1	0
	80	½	1
	400	1	1
110 to 115°C	4	½	1
	4	1	1
	80	½	2
	400	1	1
120°C	4	½	1
	4	1	1
	80	½	1
	400	1	1
125°C	4	½	2
	4	1	2

Fig. 9 shows, for comparison with Figs. 2 and 8, a board considered perfectly cleaned (cleanliness grade 0).

CONCLUSIONS

Careful consideration must be given by board assemblers to the choice of solvent for post-assembly cleaning of printed-wiring boards. The use of a product with insufficient solvency will result in incomplete removal of residues, particularly activator residues; an aggressive solvent, while dealing effectively with residues, can have a severely deleterious effect on many of the plastics and lacquers used for component encapsulation. (Fig. 10 shows component damage typical of that caused by the use of a solvent containing dichloromethane.)

The solvent must be sufficiently agitated, thermally or ultrasonically, to dislodge the residue of the flux used, without damage to components. The choice of solvent and cleaning process will therefore be partially dependent on the particular flux whose residue is to be removed. The soldering conditions (particularly the pre-heating temperature) must also be taken into account, and control should be exercised over the storage time between soldering and cleaning.

It has not been possible in this article to examine all the available cleaning systems, nor to determine all the conditions governing their effective use. When a board assembler approaches a cleaning systems supplier for guidance his application will be discussed in detail, and it is normal for proving trials of cleaning equipment to be undertaken before a decision is made. In this respect Mullard Limited wish to acknowledge with gratitude the help given by Du Pont de Nemours International S.A., by Kerry Ultrasonics Limited (a Du Pont Approved Systems Manufacturer), and by ICI Limited, Mond Division, suppliers of both solvents and plant.

Investigations into the effects on Mullard components of flux removal processes, by Mullard Limited in conjunction with cleaning systems suppliers, are continuing. In the development of new materials for component encapsulation, lacquering, and marking, the effects of cleaning are a major consideration. Thus the compatibility of Mullard components with the most effective cleaning processes will be maintained and, where possible, improved.

This article has examined only the compatibility with cleaning processes of Mullard resistors and capacitors. Printed-wiring boards to be cleaned generally include a much wider range of components, active (transistors, diodes, integrated circuits) and passive (variable resistors and capacitors, wound components). The compatibility of all these devices with the various proprietary cleaning systems has not yet been fully assessed: when information becomes available, it is hoped that a further article will be published.

REFERENCES

1. Clementson, J. J., Gilsing, C. P. G. and Pol, G. H., 'The Compatibility of Electronic Components with Fluorocarbon Solvents in Cleaning Processes', paper presented at the Internepcon Europa Conference, Brussels, June 1973, jointly by ICI Limited (Mond Division), Solvents Marketing Department, and N.V. Philips' Gloeilampenfabrieken, Electronic Components and Materials Division.
2. Barrie, R., 'Soldering and Solderability of Electronic Components', **Mullard Technical Communications,** Vol. 9, No. 81, May 1966, pp. 2 to 9.
3. Clay, W. M., A.R.I.C., 'Cleaning Problems associated with The Manufacture of Printed Circuit Boards', paper presented to the Institute of Metal Finishing (Printed Circuit Group) Symposium, October 1965, by ICI Limited (Mond Division).
4. Weeks, R. D., 'Solvents and their effects on capacitors', **Electronic Components,** 10th March 1972.

Deflection system design for 110° shadowmask tubes

J. Kaashoek
Philips Radio and Television Component Design Laboratory

UDC 621.397.334

Convergence and beam landing requirements impose far greater demands on the deflection system for a 110° shadowmask tube than on that for a 90° tube. Formerly, convergence errors on a 110° tube were corrected with a four-pole field created by injecting a difference current into the line deflection coils. However, although the electron-optical characteristics of such a system are favourable, circuit complexity is greatly increased. Analysis of the relations between coil geometry, deflection field distribution, and deflection errors shows that it is possible to achieve comparable results by suitable design of the deflection coils themselves. With the aid of recent refinements in winding technique, a saddle-yoke deflection assembly (types AT1062 and AT1063) has been developed for 110° tubes which confirms the predictions of theory. Driven by comparatively simple circuits, it gives a picture of comparable quality to that obtainable with 90° deflection, both convergence and beam landing being well within acceptable limits even at the corners of the screen.

INTRODUCTION

In any television picture tube, monochrome or colour, the raster is required to be rectangular and uniformly sharp over the whole screen. Colour reproduction in a three-gun shadowmask tube, however, imposes two additional electron-optical requirements, namely correct beam landing and correct convergence.

The beam landing requirement governs the angles of the three electron beams relative to the shadowmask and to each other. After passing through a hole in the mask, each beam must land on a phosphor dot of the colour to which it corresponds. If any one of the beam angles is incorrect, mislanding will occur and colour rendition will be impaired. To satisfy the equally important convergence requirement, all three beams must converge to a single point everywhere on the screen. If they do not, the images in the three colours will not coincide and disturbing fringes will be observed at transitions of brightness or hue.

The greater the deflection angle, the more difficult it is to satisfy all these, sometimes conflicting, requirements (raster shape, sharpness, beam landing, and convergence). The beam landing and convergence requirements in particular are so severe that they completely dominate the design of the deflection unit, even for a 90° tube. For a 110° tube, they are even more severe. Therefore, in all cases, special circuit techniques have to be adopted to correct errors in raster formation.

In addition to the electron-optical problems associated with deflecting three beams instead of one, there are geometric differences between a shadowmask tube and an ordinary black-and-white tube that affect the design of the deflection unit. Owing to the comparatively large area occupied by the triangular array of beams, the neck-cone transition needs to be given a larger radius to prevent neck-shadowing. This increases the volume of the deflection space and correspondingly reduces the deflection sensitivity. Furthermore, the deflection unit needs to be movable along the axis of the tube for colour purity adjustment. In providing for this movement, allowance must be made for a tolerance of about 8mm in the position of the neck-cone transition. Together these factors impose rather strict limits on the axial length of the deflection unit. In addition, the deflection unit must be flared over part of its length to fit the contours of the tube.

ELECTRON-OPTICAL GEOMETRY

Convergence

A deflection field not only bends the electron beams but to some extent also focuses them. It is the latter action that gives rise to convergence errors. To explain what these errors are and how they come about, we shall consider a conical pencil of beams which, in the absence of a deflection field, converges on the centre of the screen. From the behaviour of such a pencil under the influence of a deflection field, we can draw conclusions about the behaviour of the three individual beams in a shadow-mask tube.

Curvature of the image field and isotropic astigmatism

In general, the focusing action of a deflection field differs in the horizontal and vertical planes (see Fig. 1). On what

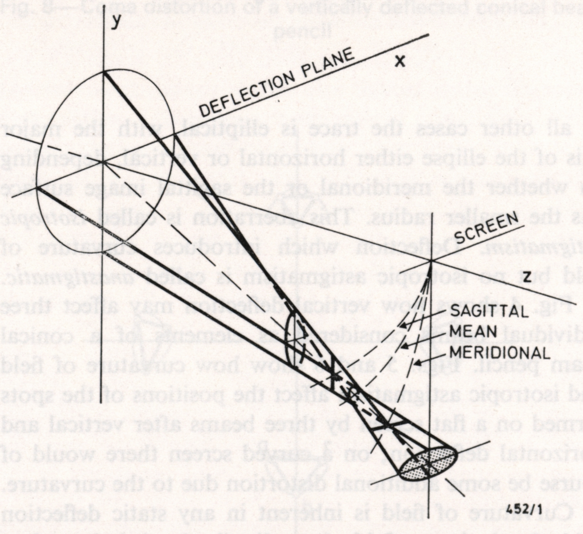

Fig. 1—Isotropic astigmatism due to vertical deflection. On the sagittal image surface, the trace of a conical beam pencil is a vertical line; on the meridional image surface, it is a horizontal line; on the mean image surface, it is a circle; and on a flat screen, it is an ellipse

is known as the *sagittal image surface*, the trace of a conical beam pencil is a line parallel to the direction of deflection; and on what is known as the *meridional image surface*, it is a line perpendicular to the direction of deflection. In between, on the *mean image surface*, the trace is circular. The radius of curvature of the mean image surface, which is approximately equal to the effective length of the deflection field, is considerably shorter than that of the screen and, with a given construction of deflection unit, cannot be changed.

An important design consideration is that the curvature radii of the sagittal and meridional image surfaces depend on the distribution of the deflection field, and particularly on the field pattern in the region closest to the screen. If the lines of force curve inward (as in Fig. 2a), the radius of the meridional surface is large and that of the sagittal surface small; if they curve outward (Fig. 2b) the opposite is true. A special case, which is known as *curvature of the image field*, is when all three surfaces coincide. The trace of the beam pencil on a flat screen is then circular (Fig. 3).

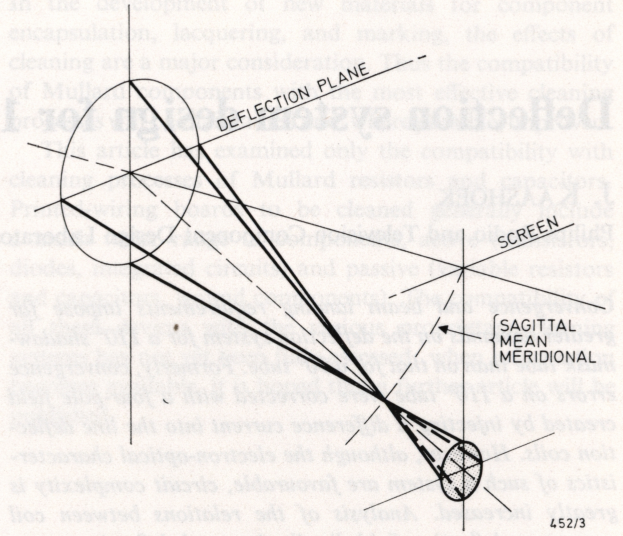

Fig. 3—When the three image surfaces coincide (curvature of the image field), the trace of a conical beam pencil on a flat screen is circular

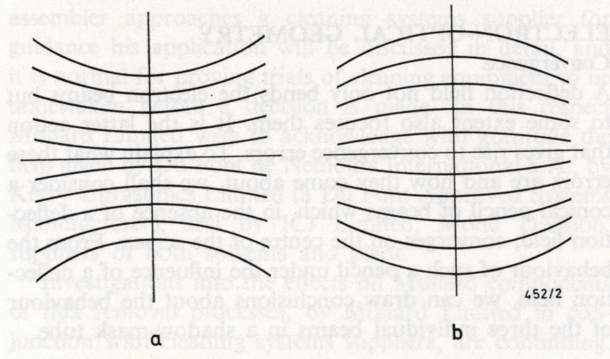

Fig. 2—A deflection field with inward curving lines of force (a) increases the radius of the meridional image surface; one with outward curving lines of force (b) increases the radius of the sagittal image surface

In all other cases the trace is elliptical, with the major axis of the ellipse either horizontal or vertical, depending on whether the meridional or the sagittal image surface has the smaller radius. This aberration is called *isotropic astigmatism.* Deflection which introduces curvature of field but no isotropic astigmatism is called *anastigmatic.*

Fig. 4 shows how vertical deflection may affect three individual beams considered as elements of a conical beam pencil. Figs. 5 and 6 show how curvature of field and isotropic astigmatism affect the positions of the spots formed on a flat screen by three beams after vertical and horizontal deflection; on a curved screen there would of course be some additional distortion due to the curvature.

Curvature of field is inherent in any static deflection field; that is, in any field whose distribution is independent of its intensity. Hence, it is impossible to design such a field in which three statically converged beams will remain converged on a flat screen throughout all angles of deflection. The practical alternative is to provide means for varying the angles between the three beams in accordance with the deflection; this is known as *dynamic convergence.*

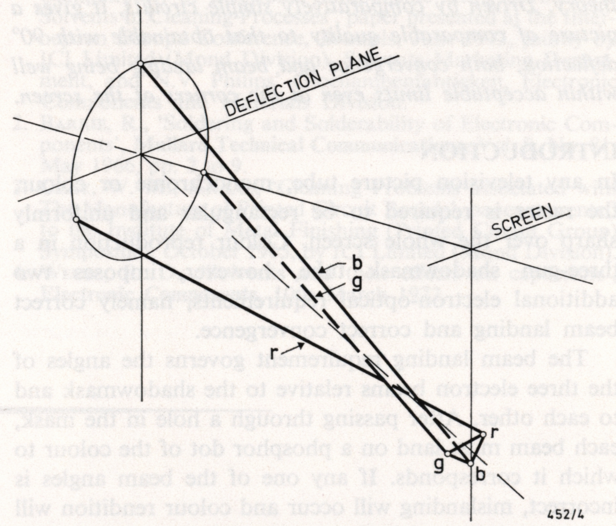

Fig. 4—Effect of curvature of the image field and isotropic astigmatism on the spots formed by three equally spaced beams after vertical deflection; r, g, and b correspond to the red, green, and blue beams in a shadowmask tube

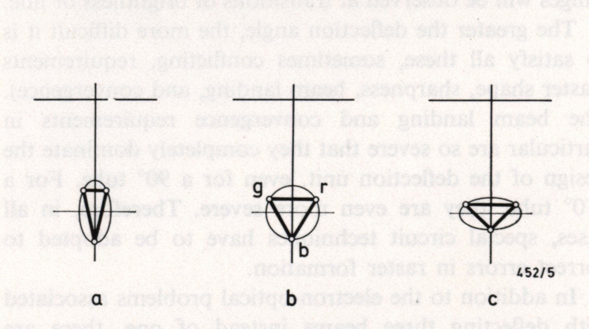

Fig. 5—Distortion due to vertical deflection; (a) and (c) show the effects of isotropic astigmatism and curvature of the image field and (b) shows the effect of curvature of the image field alone. Ideally, all three spots should coincide

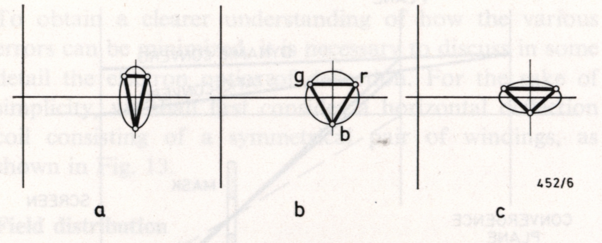

Fig. 6—Distortion due to horizontal deflection; (a) and (c) show the effects of isotropic astigmatism and curvature of the image field and (b) shows the effect of curvature of the image field alone. Ideally, all three spots should coincide

Anisotropic astigmatism

When a beam pencil is deflected both horizontally and vertically, the defocusing effect of the combined fields is generally greater than the sum of their individual effects. The increment is an oblique distortion known as *anisotropic astigmatism.* As shown in Fig. 7, it displaces the ends of the ellipse axes perpendicularly to the planes formed by the individual beams and the axis of the beam pencil.

Anisotropic astigmatism can be the cause of quite large convergence errors. This is troublesome because the dynamic convergence circuits can be kept reasonably simple only if the corrections required in the corners of the screen can be obtained by merely adding together those required at the ends of the axes. In general, that can be done only if there is no anisotropic astigmatism. However, calculation and measurements have shown that it is not possible to eliminate both isotropic and anisotropic astigmatism.

Thus, we must be prepared to accept a certain amount of isotropic astigmatism and also accept that dynamic correction of it will have an unfavourable effect on beam landing and hence on colour purity (see Beam Landing, page 18).

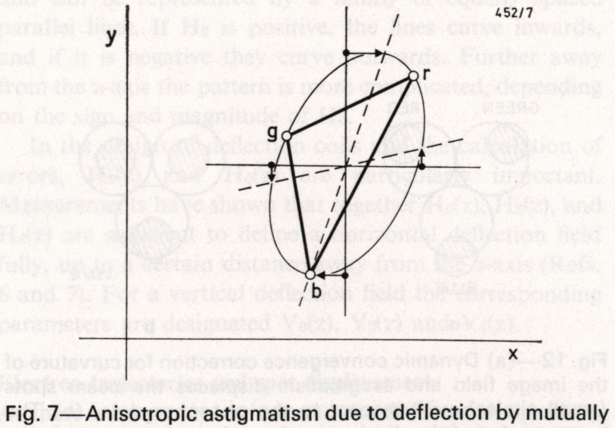

Fig. 7—Anisotropic astigmatism due to deflection by mutually perpendicular fields. The solid dots show where the ends of the ellipse axes would lie if there were curvature of the image field and isotropic astigmatism but no anisotropic astigmatism

Coma

Another convergence error caused by deflection is *coma.* A more or less typical example of its effect on the trace of a conical beam pencil on a flat screen is given in Fig. 8. At best, coma can be no more than partially compensated by the usual radial dynamic convergence corrections.

One common example of coma, resulting from horizontal deflection, is a lateral displacement of the blue beam with respect to red and green. To counteract this error, a lateral dynamic correction for blue has to be introduced. Another example is a difference between the convergence errors at the top and bottom of the screen. To counteract this error, the field frequency radial corrections have to be made asymmetric. Fig. 9 shows the (uncorrected) shapes of the spot triangles formed by three beams after deflection by horizontal and vertical fields having some astigmatism and coma.

Since astigmatism and coma depend on the field distribution in quite different ways, they are likely to impose conflicting requirements on the design of the deflection system. A compromise is therefore necessary.

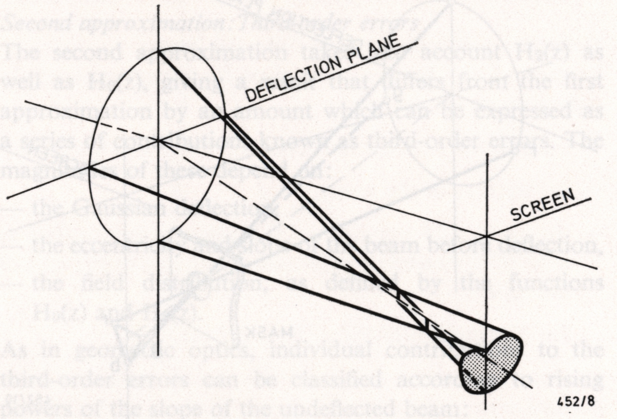

Fig. 8—Coma distortion of a vertically deflected conical beam pencil

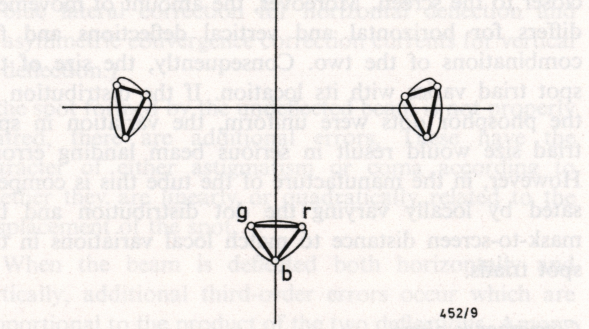

Fig. 9—Distortions due to the combined effects of astigmatism and coma

Beam landing

Before the beams reach the screen, they must pass through the holes in the shadow-mask, each beam at such an angle that it will strike a phosphor dot of the correct colour. Since the holes in the mask are smaller than the phosphor dots, there is some margin for error in the beam angles; but if any beam lands even partly beyond the edge of the correct dot a colour error will result.

The angles depend not only on the eccentricity and static convergence of the three electron guns but also on the effects of deflection and dynamic convergence. To understand how each of these affects the beam landing, we must consider the *deflection plane*, the *deflection points*, and the *convergence plane*.

Deflection plane and deflection points

The deflection plane is the plane in which the action of the deflection field can be considered to be concentrated. The deflection points are the three points in the deflection plane from which the beams appear to originate. The spot triad on the screen is the inverted image of the deflection points formed by a hole in the shadow-mask. At small deflection angles, the geometrical relationship between the spot triad and the deflection points can be regarded as constant (Fig. 10). However, as the angle increases, the deflection plane tends to move, usually closer to the screen. Moreover, the amount of movement differs for horizontal and vertical deflections and for combinations of the two. Consequently, the size of the spot triad varies with its location. If the distribution of the phosphor dots were uniform, the variation in spot triad size would result in serious beam landing errors. However, in the manufacture of the tube this is compensated by locally varying the dot distribution and the mask-to-screen distance to match local variations in the spot triads.

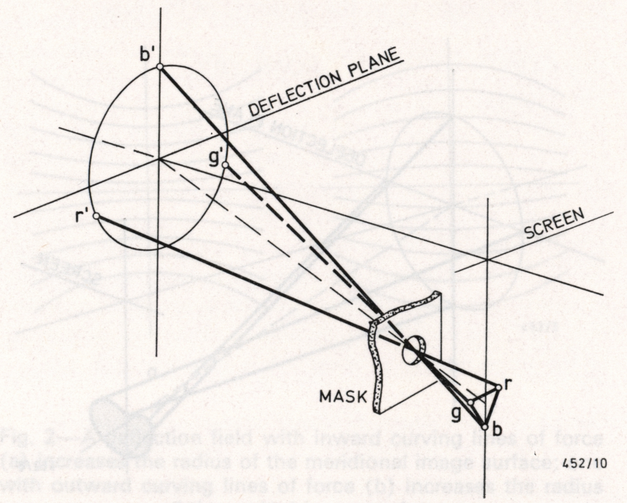

Fig. 10—Relationship between the deflection points r', g', b', the shadowmask, and the spot triad r, g, b (schematic)

Convergence plane

Corrections for curvature of field and astigmatism are made by means of a separate magnetic field called the convergence field. The action of this field can be considered to be concentrated in a plane between the deflection plane and the electron guns. As the corrections applied by the convergence field pre-deflect the beams outwards, they result in an enlargement of the deflection point triangle and the corresponding spot triad (see Fig. 11). This too can be compensated during manufacture of the tube, but only to the extent that the pre-deflection is similar for all three beams (curvature of field).

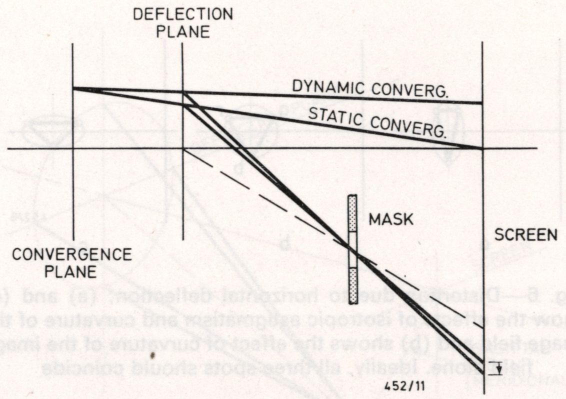

Fig. 11—Dynamic convergence pre-deflects the beams outwards, enlarging the spot triads. (For the sake of clarity only one beam is shown; relative angles and spacings are grossly exaggerated)

If there is isotropic astigmatism (as in Figs. 5a and 6a), the correction required for the blue beam is considerably greater than for the red or green. After convergence, the position of the spot triad relative to the phosphor dots is as shown in Fig. 12a. By adjusting the mask-to-screen distance to compensate the common part of the misplacement, a situation as shown in Fig. 12b can be achieved. If the blue spot still oversteps the edge of the blue phosphor dot, a colour error will result.

Anisotropic astigmatism can cause similar errors. If these also have to be corrected by the convergence field, it is obvious that the colour purity requirement will set a very strict limit to the amount of either type of astigmatism that can be tolerated initially.

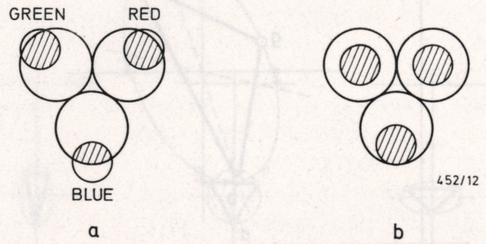

a

b

Fig. 12—(a) Dynamic convergence correction for curvature of the image field and astigmatism displaces the beam spots (small circles) with respect to the phosphor dots. (b) The common part of the displacement can be compensated in the manufacture of the tube, but a displacement of the blue dot due to isotropic astigmatism remains

ESSENTIALS OF DEFLECTION ERROR THEORY

To obtain a clearer understanding of how the various errors can be minimized, it is necessary to discuss in some detail the electron optics of deflection. For the sake of simplicity, we shall first consider a horizontal deflection coil consisting of a symmetrical pair of windings, as shown in Fig. 13.

Field distribution

In the neighbourhood of the z-axis, the distribution of a symmetrical field can be expressed by a series development in x and y. If terms of the sixth and higher order are neglected, the field strength in the plane y = 0 at any point along the z-axis is given by:

$$H(z) = H_0(z)+H_2(z)x^2+H_4(z)x^4,$$

where $H_0(z)$ is the field strength along the z-axis itself, and $H_2(z)$ and $H_4(z)$ are measures of its variation in the x-direction (Refs. 1 to 6).

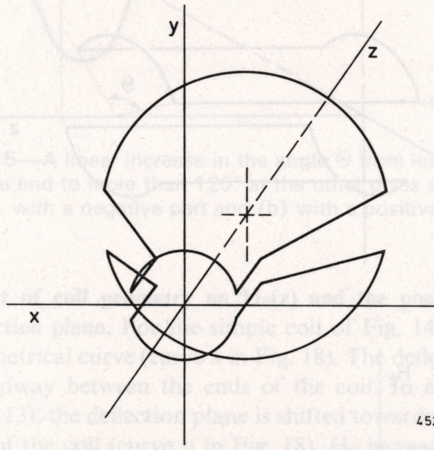

Fig. 13—Simplified outline of a horizontal deflection coil consisting of paired windings with a constant-diameter section followed by a flared section. Electrons enter along the z-axis and are deflected parallel to the x-axis

If both H_2 and H_4 are zero at any value of z, the field strength perpendicular to the axis at that point is constant and can be represented by a family of equally spaced parallel lines. If H_2 is positive, the lines curve inwards, and if it is negative they curve outwards. Further away from the z-axis the pattern is more complicated, depending on the sign and magnitude of H_4.

In the design of deflection coils and the calculation of errors, $H_2(z)$ and $H_4(z)$ are particularly important. Measurements have shown that together $H_0(z)$, $H_2(z)$, and $H_4(z)$ are sufficient to define a horizontal deflection field fully, up to a certain distance away from the z-axis (Refs. 6 and 7). For a vertical deflection field the corresponding parameters are designated $V_0(z)$, $V_2(z)$ and $V_4(z)$.

Electron trajectories and spot displacement

As there is no general solution to the differential equations for electron trajectories in a magnetic field, exact calculation of the deflection errors is not possible. Instead, a method of successive approximation based on a series expansion has to be used. In the first approximation, all terms higher than first degree are neglected, in the second approximation terms higher than third degree, and in the third approximation terms higher than fifth degree. Approximations of higher orders than the third do not yield a worth-while improvement in accuracy.

First approximation: Ideal deflection

For horizontal deflection, the first approximation is found by twice integrating $H_0(z)$ over the distance from the electron gun to the screen and multiplying the result by a proportionality factor which, amongst other things, takes account of the potential difference between cathode and screen. This gives the ideal, or so-called Gaussian deflection, which is proportional to the strength of the deflection field and, hence, to the current through the coil. Information obtained from this approximation concerning the point at which the beam strikes the screen is accurate only for very small angles of deflection. The spot formed at the point of impact is no different from that formed by an undeflected beam.

Second approximation: Third-order errors

The second approximation takes into account $H_2(z)$ as well as $H_0(z)$, giving a result that differs from the first approximation by an amount which can be expressed as a series of contributions known as third-order errors. The magnitudes of these depend on:

- the Gaussian deflection,
- the eccentricity and slope of the beam before deflection,
- the field distribution, as defined by the functions $H_0(z)$ and $H_2(z)$.

As in geometric optics, individual contributions to the third-order errors can be classified according to rising powers of the slope of the undeflected beam:

- *Raster distortion* is independent of the slope but proportional to the third power of the deflection angle.
- *Curvature of field* and *isotropic astigmatism* are proportional to the slope and to the square of the Gaussian deflection. (These are the errors that call for parabolic convergence corrections.)
- *Coma* is proportional to the deflection angle and to the square of the slope. (This is the error that necessitates blue lateral correction for horizontal deflection and asymmetric convergence correction currents for vertical deflection.)

If the spot formed by the undeflected beam is not properly centred, there are additional errors. These have the character of either astigmatism or coma according to whether they are linearly or quadratically related to the misplacement of the spot.

When the beam is deflected both horizontally and vertically, additional third-order errors occur which are proportional to the product of the two deflections. Among these may be pincushion or barrel distortion, as well as anisotropic astigmatism.

Third approximation: Fifth-order errors

The third approximation, which takes into account $H_4(z)$ and $V_4(z)$, gives a result that differs from the second approximation by a series of contributions known as fifth-order errors. In each term the powers of the beam slope and the Gaussian deflection add up to five. For the fairly small slopes encountered in practice, however, those terms can be disregarded in which the third or a higher power of the slope occurs. As before, the remainder can be classified according to ascending powers of the slope:

— *Fifth-order raster distortion* (which includes linearity errors as well as barrel and pincushion distortion) is independent of the slope but proportional to the fifth power of the horizontal or vertical deflection, or to fifth degree products of the two deflections.

— *Fifth-order astigmatism* is proportional to the slope and to the fourth power of the deflection. It includes an *isotropic* part proportional to the fourth power of either the horizontal or the vertical deflection, and an *anisotropic* part proportional to fourth degree products of the two deflections.

Fifth-order coma is proportional to the square of the slope and to third degree products of the two deflections.

Deflection coil geometry and deflection errors

In general, the factors that affect the magnitudes of the deflection errors are:

— the distance between the deflection plane and the screen;

— the flatness of the screen;

— the slope and position of the electron beams (hence, their positions relative to each other and to the axis of the tube);

— the distribution of the deflection field.

However, once the design of the picture tube has been decided upon, all except the last of these are fixed. Thus, the only practical way to keep errors within allowable limits is to control the distribution of the field. This depends not only on the geometry of the deflection coil as a whole but also on the geometries of the individual turns that make up its windings.

The relationship between coil geometry and deflection errors is so complicated that it is best considered in two parts.

1) The relationship between coil geometry and field distribution,

2) The relationship between field distribution and deflection errors.

The results of such an analysis can be summarized in fairly simple terms from which it is possible to derive some important principles of deflection coil design.

Coil Geometry and Field Distribution

The theoretical treatment of deflection errors often takes as a starting point a homogeneous deflection field. In practice, however, complete homogeneity is neither easy to obtain nor does it always give the best results and certain departures from it are often necessary. It is more to the point, therefore, to start by considering how each turn in a coil contributes to the field as a whole.

Effect of coil geometry on $H_2(z)$ In a symmetrical coil consisting of two single turns (Fig. 14a), $H_2(z)$ depends on the angle Θ subtended by each turn (Fig. 14b).

—If Θ = 120°, H_2 is everywhere close to zero.

—If Θ > 120°, H_2 is predominantly positive.

—If Θ < 120°, H_2 is predominantly negative.

The $H_2(z)$ curve for a multiple-turn coil can be found by summation of the contributions of each turn.

Varying the angle Θ along the length of the coil correspondingly varies the form of $H_2(z)$. A linear variation, for example from $\Theta < 120°$ at one end of the coil to $\Theta > 120°$ at the other, as in Fig. 15a, gives an H_2 curve like that of Fig. 15b. With the aid of a computer, the effect of more complicated coil shapes, such as that of Fig. 13, can readily be worked out. Figs. 16 and 17 give some examples.

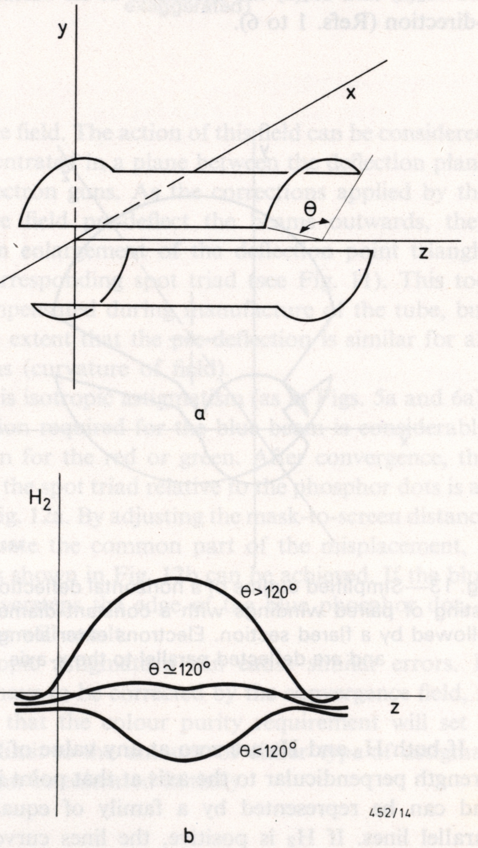

Fig. 14—In a constant-diameter coil consisting of two symmetrical, single-turn windings (a), the angle Θ determines the shape of the $H_2(z)$ curve (b)

The extra degree of freedom that variation of the angle Θ gives to the coil designer enables him to influence coma more or less independently of astigmatism. As we shall see later, this is but one aspect of the importance of Θ as a design parameter.

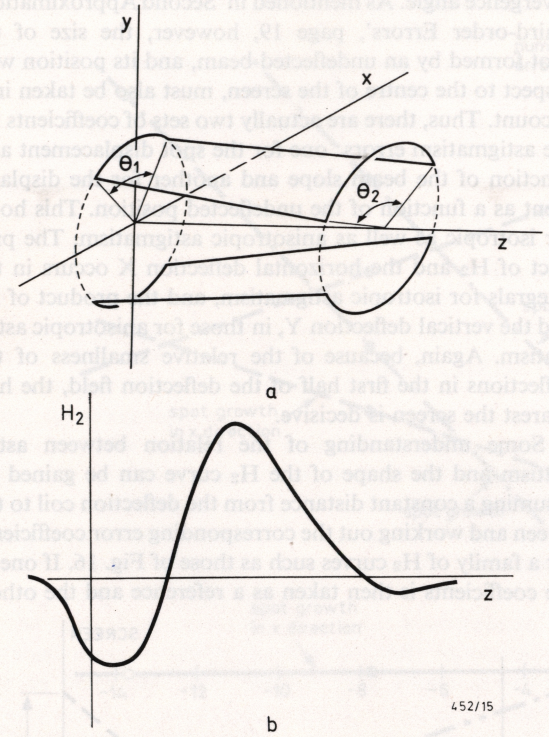

Fig. 15—A linear increase in the angle Θ from less than 120° at one end to more than 120° at the other gives an $H_2(z)$ (a) with a negative part and (b) with a positive part

Effect of coil geometry on $H_0(z)$ and the position of the deflection plane. For the simple coil of Fig. 14, $H_0(z)$ is a symmetrical curve (curve a in Fig. 18). The deflection plane is midway between the ends of the coil. In a flared coil (Fig. 13), the deflection plane is shifted towards the narrow end of the coil (curve b in Fig. 18). H_0 increases with the angle Θ, so in coils with varying Θ the deflection plane moves towards the region where Θ is greatest. As the position of the horizontal and vertical deflection planes relative to each other has an effect on the beam landing, this is a factor of some importance in the design of deflection systems for shadowmask tubes.

Effect of coil geometry on $H_4(z)$. Fig. 19 shows how the calculated value of H_4 as a function of z varies with Θ in a flared coil. It can be seen that there is a distinct relationship between the value of Θ and the maximum absolute value of H_4.

Field Distribution and Deflection Errors

In the theory of deflection errors, the relationship between field distribution and aberrations is expressed in terms of error coefficients. These are proportionality factors in the expressions for the third and fifth order errors discussed earlier. Most of them contain the sum of two or more integrals.

One or more of the integrals in each coefficient relates solely to $H_0(z)$ and/or $V_0(z)$. Since, in a coil of given shape and size, these are affected to only a limited extent by changes in the turns distribution, their contribution to the error coefficients can be regarded as constant. The remaining integrals for the third-order coefficients contain

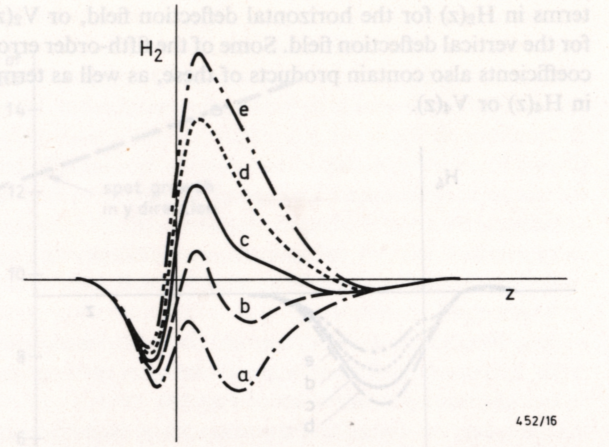

Fig. 16—Effect of the angle Θ on $H_2(z)$ in a flared coil of the type shown in Fig. 13
(a) Θ = 110° (b) Θ = 115° (c) Θ = 120°
(d) Θ = 125° (e) Θ = 130°

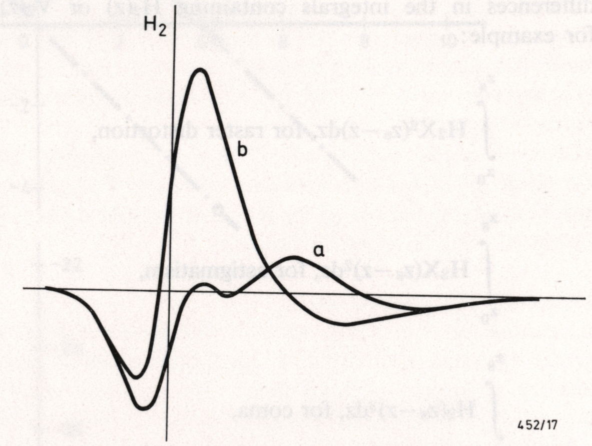

Fig. 17—Effect of lengthwise variation of the angle Θ on $H_2(z)$ in a flared coil
(a) Θ increases from 110° to 130°
(b) Θ decreases from 130° to 110°

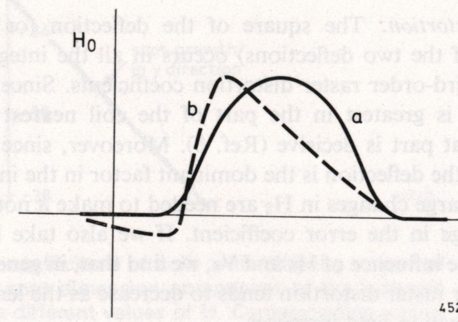

Fig. 18—Effect of flare on $H_0(z)$
(a) Constant-diameter coil (Fig. 14a)
(b) Flared coil (Fig. 13)

terms in $H_2(z)$ for the horizontal deflection field, or $V_2(z)$ for the vertical deflection field. Some of the fifth-order error coefficients also contain products of these, as well as terms in $H_4(z)$ or $V_4(z)$.

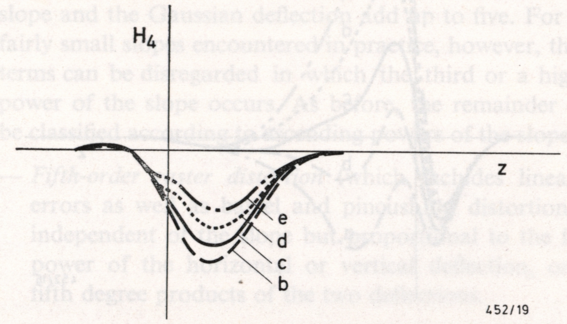

Fig. 19—Effect of the angle Θ on $H_4(z)$ in a flared coil (cf. Fig. 16)
(b) Θ = 115° (d) Θ = 125°
(c) Θ = 120° (e) Θ = 130°

Third-order errors

The third-order error coefficients are distinguished by differences in the integrals containing $H_2(z)$ or $V_2(z)$; for example:

$$\int_{z_0}^{z_s} H_2X^2(z_s-z)dz, \text{ for raster distortion,}$$

$$\int_{z_0}^{z_s} H_2X(z_s-z)^2dz, \text{ for astigmatism,}$$

$$\int_{z_0}^{z_s} H_2(z_s-z)^3dz, \text{ for coma,}$$

in which z_0 is at the origin of the beam, z_s is at the screen, and X is the lateral deflection of the beam as a function of z. Fig. 20 shows a typical example of how the field parameter H_2, the deflection X, and the product H_2X vary over the region of integration. Since the quantity (z_s-z) changes only slightly in the interval where H_2 and H_2X are significant, it can be regarded as constant for purposes of qualitative discussion.

Raster distortion: The square of the deflection (or the product of the two deflections) occurs in all the integrals for the third-order raster distortion coefficients. Since the deflection is greatest in the part of the coil nearest the screen, that part is decisive (Ref. 8). Moreover, since the square of the deflection is the dominant factor in the integral, quite large changes in H_2 are needed to make a noticeable change in the error coefficient. If we also take into account the influence of H_0 and V_0, we find that, in general, third-order raster distortion tends to decrease as the length of the deflection field increases.

Astigmatism: The size and position of the spot formed by a deflected beam depend on the slope of the beam and its divergence angle. As mentioned in 'Second Approximation: Third-order Errors', page 19, however, the size of the spot formed by an undeflected beam, and its position with respect to the centre of the screen, must also be taken into account. Thus, there are actually two sets of coefficients for the astigmatism errors: one for the spot displacement as a function of the beam slope and another for the displacement as a function of the undeflected position. This holds for isotropic as well as anisotropic astigmatism. The product of H_2 and the horizontal deflection X occurs in the integrals for isotropic astigmatism, and the product of H_2 and the vertical deflection Y, in those for anisotropic astigmatism. Again, because of the relative smallness of the deflections in the first half of the deflection field, the half nearest the screen is decisive.

Some understanding of the relation between astigmatism and the shape of the H_2 curve can be gained by assuming a constant distance from the deflection coil to the screen and working out the corresponding error coefficients for a family of H_2 curves such as those of Fig. 16. If one of the coefficients is then taken as a reference and the others plotted against it, there is found to be a linear relation between them (see Fig. 21). This implies that it is not practicable to influence isotropic astigmatism and anisotropic astigmatism independently of each other by varying the turns distribution of the deflection coil. Adjusting H_2 so as to give one of the coefficients a desired value automatically fixes the values of the other coefficients as well.

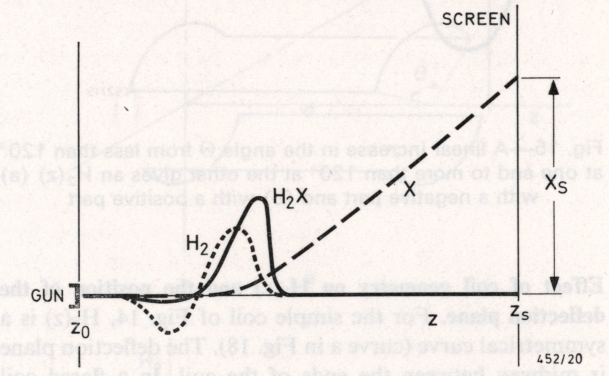

Fig. 20—Typical variations of the field parameter H_2, the deflection X, and the product H_2X as functions of z; these quantities occur in the integrals for the third-order error coefficients

An interesting feature is that for coils of the type shown in Fig. 14, there is also a linear relationship between astigmatism and the angle Θ, which facilitates the application of Θ as a design parameter.

For the deflection field to be free of isotropic astigmatism, both the coefficients relating to beam slope must be equal; according to Fig. 21 the anisotropic astigmatism will then be negative. On the other hand, for the field to be free of anistropic astigmatism, the horizontal deflection coil has to be designed so that there is strong isotropic astigmatism, particularly in the direction perpendicular to the deflection.

If raster distortion coefficients are plotted against one of the astigmatism coefficients in the manner of Fig. 21, they too turn out to be straight lines. This implies that with the

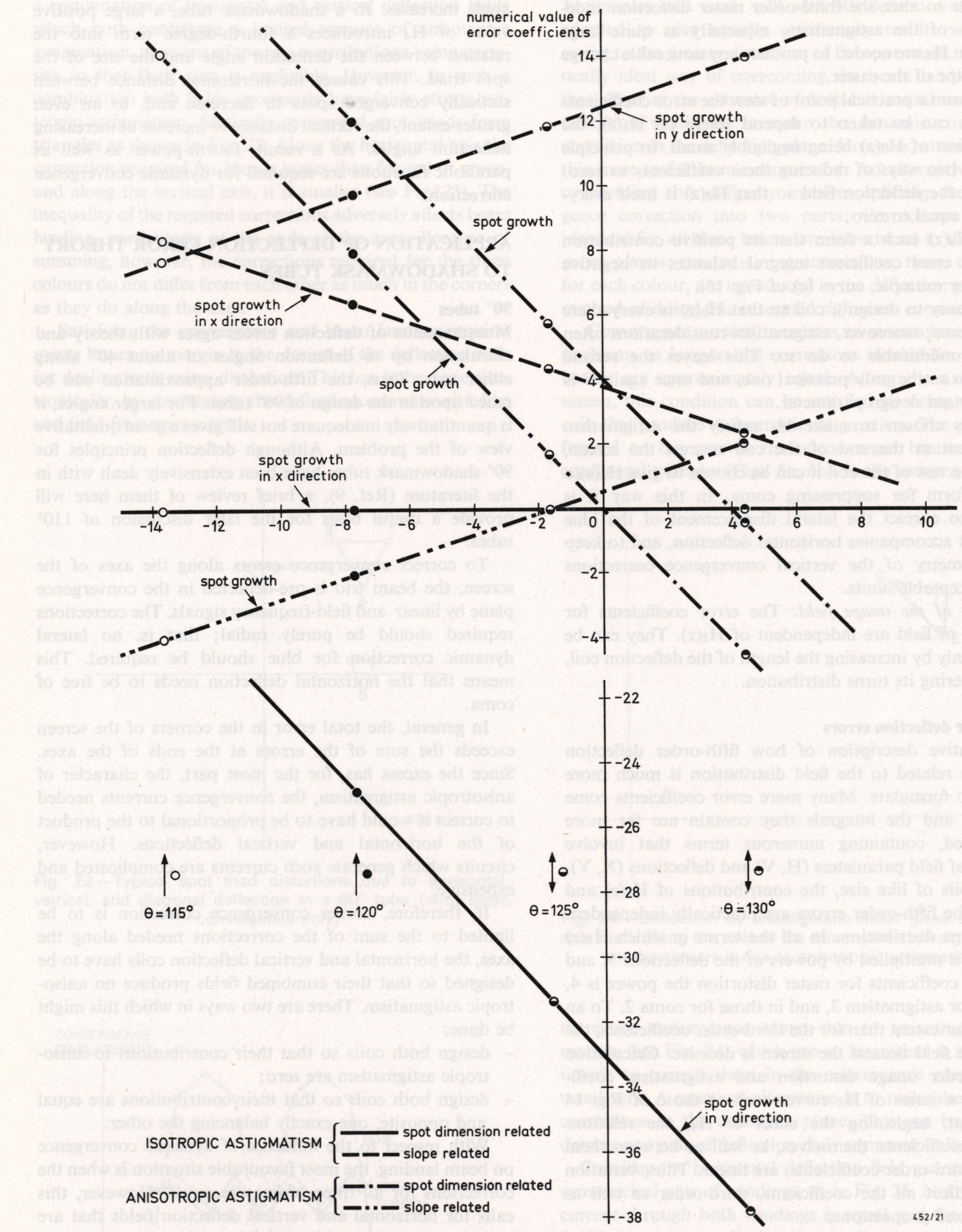

Fig. 21—The linear relationship between corresponding error coefficients of coils with differing values of the angle Θ. The spot growth in the X direction due to the spot dimension component of the isotropic astigmatism error is plotted along the horizontal axis for five different values of Θ. Corresponding values of error coefficients for spot growths in the X and Y directions due to the two components (spot dimension-related and slope-related) of both isotropic and anisotropic astigmatism are plotted along the vertical axis

relatively short deflection coils used in practice it is virtually impossible to alter the third-order raster distortion independently of the astigmatism, especially as quite large changes in H_2 are needed to produce any noticeable change in the shape of the raster.

Coma: From a practical point of view the error coefficients for coma can be taken to depend solely on $H_2(z)$, the contribution of $H_0(z)$ being negligibly small. In principle there are two ways of reducing these coefficients to zero:

- design the deflection field so that $H_2(z)$ is itself everywhere equal to zero;
- give $H_2(z)$ such a form that its positive contribution to the error coefficient integral balances its negative one (for example, curve (c) of Fig. 16).

It is not easy to design a coil so that $H_2(z)$ is everywhere equal to zero; moreover, astigmatism considerations often make it undesirable to do so. This leaves the second alternative as the only practical one, and once again Θ is the important design parameter.

If Θ is chosen to make H_2 satisfy the astigmatism requirement at the end of the coil nearest the screen, then in the rest of the coil it can be chosen to give $H_2(z)$ a suitable form for suppressing coma. In this way it is possible to correct the lateral displacement of the blue beam that accompanies horizontal deflection, and to keep the asymmetry of the vertical convergence corrections within acceptable limits.

Curvature of the image field: The error coefficients for curvature of field are independent of $H_2(z)$. They can be reduced only by increasing the length of the deflection coil, not by altering its turns distribution.

Fifth-order deflection errors

A qualitative description of how fifth-order deflection errors are related to the field distribution is much more difficult to formulate. Many more error coefficients come into play and the integrals they contain are far more complicated, containing numerous terms that involve products of field parameters (H, V) and deflections (X, Y).

For coils of like size, the contributions of $H_0(z)$ and $V_0(z)$ to the fifth-order errors are practically independent of the turns distribution. In all the terms in which $H_2(z)$ occurs, it is multiplied by powers of the deflections X and Y. In the coefficients for raster distortion the power is 4, in those for astigmatism 3, and in those for coma 2. To an even greater extent than for the third-order coefficients, the end of the field nearest the screen is decisive. Calculation of fifth-order image distortion and astigmatism coefficients for a series of H_2 curves such as those of Fig. 14 shows that, neglecting the effect of H_4, the relations between coefficients themselves, as well as between them and the third-order coefficients, are linear. Thus, variation H_2 will affect all the coefficients, third-order as well as fifth, in fixed proportions.

In the integrals containing $H_4(z)$ and $V_4(z)$, third and fourth powers of the deflection also occur, again emphasizing the importance of that part of the field nearest the screen. Calculation shows that there is less pincushion distortion when H_4 is positive. The effect of a positive value of H_4 on isotropic astigmatism is to increase the radius of curvature of the meridional image surface and to decrease that of the sagittal image surface as the deflection angle increases. In a shadowmask tube, a large positive value of H_4 introduces a fourth-degree term into the relation between the deflection angle and the size of the spot triad. This causes the horizontal distance between statically converged spots to decrease and, to an even greater extent, the vertical distance to increase at increasing deflection angles. As a result, fourth-power as well as parabolic functions are required for dynamic convergence correction.

APPLICATION OF DEFLECTION ERROR THEORY TO SHADOWMASK TUBES

90° tubes

Measurements of deflection errors agree with theory and calculation up to deflection angles of about 40° along either axis. Thus, the fifth-order approximation can be relied upon in the design of 90° tubes. For larger angles, it is quantitatively inadequate but still gives a good qualitative view of the problem. Although deflection principles for 90° shadowmask tubes have been extensively dealt with in the literature (Ref. 9), a brief review of them here will provide a useful basis for the later discussion of 110° tubes.

To correct convergence errors along the axes of the screen, the beam trio is pre-deflected in the convergence plane by linear and field-frequency signals. The corrections required should be purely radial; that is, no lateral dynamic correction for blue should be required. This means that the horizontal deflection needs to be free of coma.

In general, the total error in the corners of the screen exceeds the sum of the errors at the ends of the axes. Since the excess has, for the most part, the character of anisotropic astigmatism, the convergence currents needed to correct it would have to be proportional to the product of the horizontal and vertical deflections. However, circuits which generate such currents are complicated and expensive.

If, therefore, corner convergence correction is to be limited to the sum of the corrections needed along the axes, the horizontal and vertical deflection coils have to be designed so that their combined fields produce no anisotropic astigmatism. There are two ways in which this might be done:

- design both coils so that their contributions to anisotropic astigmatism are zero;
- design both coils so that their contributions are equal and opposite, one exactly balancing the other.

With respect to the influence of dynamic convergence on beam landing, the most favourable situation is when the corrections for all three beams are equal. However, this calls for horizontal and vertical deflection fields that are both anastigmatic, and in combination such fields produce strong anisotropic astigmatism. If only one of the fields were anastigmatic, the anisotropic astigmatism of the combined fields could only be reduced to zero if the other field was made so strong as to result in serious landing errors.

Obviously, a compromise has to be made. With regard to convergence and beam landing, the best compromise is a combination of horizontal and vertical deflection fields which both contribute a limited amount of anisotropic astigmatism, the signs of the two contributions being opposite so that their sum is negligible. However, in such a combination both fields necessarily have fairly strong isotropic astigmatism. Statically converged spot triads form triangles as shown in Fig. 22. Along the horizontal axis the correction required for blue is larger than for red or green, and along the vertical axis, it is smaller (see Fig. 23). The inequality of the required corrections adversely affects beam landing, particularly at the ends of the axes. Because of summing, however, the corrections required for the three colours do not differ from each other as much in the corners as they do along the axes.

Satisfying the convergence and beam landing requirements leaves no margin in the design of the deflection coils for dealing with raster distortion. This has to be done electronically, by modulating the deflection currents with line and field-frequency signals.

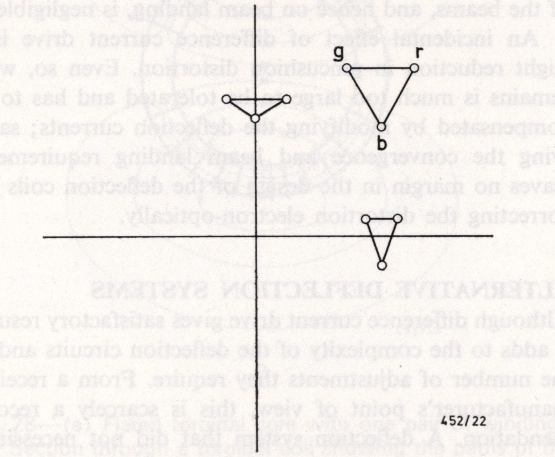

Fig. 22—Typical spot triad distortions due to horizontal, vertical, and diagonal deflection in a 90° tube (with static convergence only)

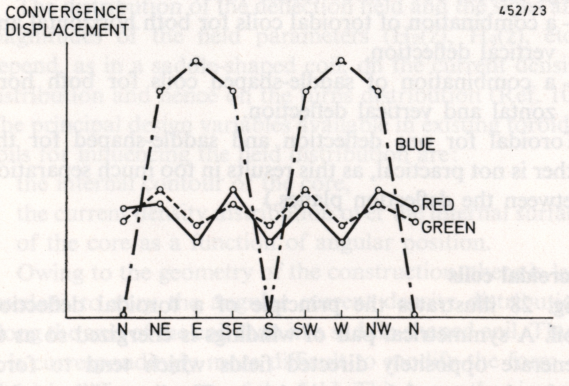

Fig. 23—Required convergence corrections (relative) as measured at points 10mm from the end of the screen of a 90° tube (random specimen)

110° tubes

Techniques that work well with 90° deflection cannot be adapted to give equally satisfactory results with 110°, owing to the greater distortion of the spot triads. A theoretically ideal way of overcoming the beam landing errors that occur at the extremes of both horizontal and vertical deflection would be to make the dynamic convergence correction in the deflection plane. However, attempts to do this have so far been unsuccessful. An alternative way of overcoming this difficulty involves splitting the convergence correction into two parts. Corrections that are identical for all three beams are introduced in the convergence planes; the remaining corrections, those that differ for each colour, are introduced in the deflection plane. The method of doing this is termed *difference current drive.*

Convergence correction creates no serious beam landing problems as long as the corrections needed for the three beams are approximately equal. Along the axes of the screen, this condition can be satisfied by using deflection coils that produce no isotropic astigmatism. The spot triads formed on the axes by the unconverged beams are then equilateral triangles (Figs. 5b, 6b). In the corners, however, there are convergence errors due to anisotropic astigmatism (see Fig. 24) which are so large that it is impractical to correct them in the convergence plane in the usual way. A practical alternative is to make the required corrections in the deflection plane. This can be done by driving one pair of deflection coils asymmetrically.

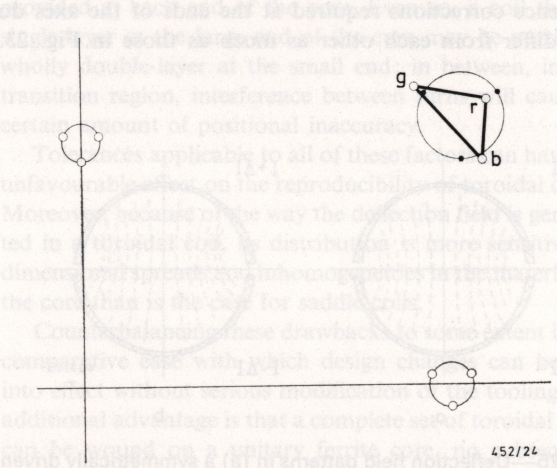

Fig. 24—Deflection by anastigmatic fields gives equilateral spot triads along the axes of the screen; the convergence error in the corners is due to anisotropic astigmatism

Consider the horizontal deflection field generated by a symmetrical pair of windings, as in Fig. 25. Normally, the current through both windings is equal and the resulting field has two perpendicular planes of symmetry (Fig. 25a). But, if the current through the upper winding is increased and that through the lower winding is decreased by the same amount, the field becomes asymmetric, as in Fig. 25b. As a result, the positions of the horizontally deflected, statically converged, spots are modified, as shown in Fig. 26. For horizontal components of beam slope, vertical spot displacements are introduced, and for vertical components, horizontal displacements are introduced. Thus, the effect very much resembles anisotropic astigmatism, except that the errors in spot position are proportional only to the horizontal deflection instead of to the product of the two deflections. However, if the current difference between the two windings is itself made proportional to the vertical deflection, the resemblance can be made complete. Thus, by applying a difference current of the correct polarity to the windings of the horizontal deflection coil, and by suitably modulating it at the frequency of the vertical deflection (field frequency), it is possible to obtain very good compensation for anisotropic astigmatism. (The same effect could be obtained by applying a line-frequency modulated difference current to the vertical deflection coil, but from a circuit design point of view this would be somewhat more complicated.)

In practice, the best results are obtained if the vertical deflection coil is not completely anastigmatic and the difference current is made proportional to slightly more than the first power of the vertical deflection current (see Fig. 27).

In a 110° tube with difference current drive, the convergence corrections required at the ends of the axes do not differ from each other as much as those in Fig. 23.

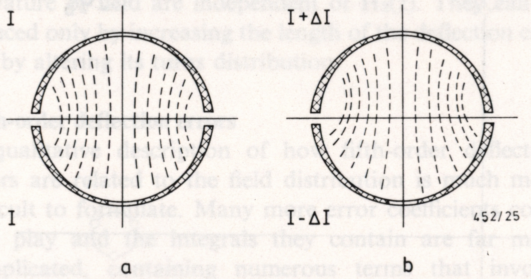

Fig. 25—Deflection field patterns in (a) a symmetrically driven coil and (b) an asymmetrically driven coil; I is the nominal drive current and ΔI is the difference current

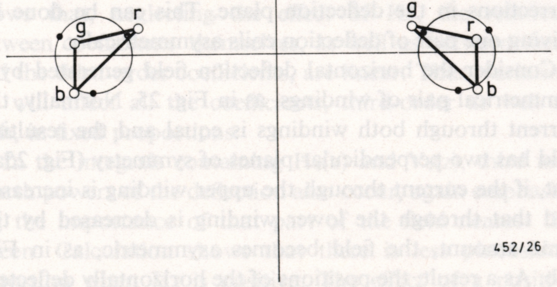

Fig. 26—Effect of asymmetrical horizontal deflection coil drive on the spot triads (static convergence only)

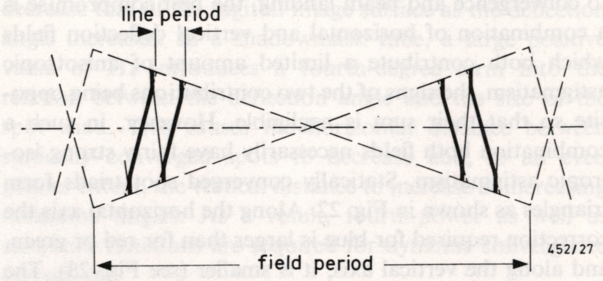

Fig. 27—Field-frequency modulation of the difference current I applied to the horizontal deflection coil

Thus, they have a relatively smaller effect on beam landing than in a 90° tube with conventional deflection and convergence. Furthermore, since the additional corrections needed in the corners of the screen are applied in the deflection plane rather than the convergence plane, the effect of the convergence corrections on the relative angles of the beams, and hence on beam landing, is negligible.

An incidental effect of difference current drive is a slight reduction in pincushion distortion. Even so, what remains is much too large to be tolerated and has to be compensated by modifying the deflection currents; satisfying the convergence and beam landing requirements leaves no margin in the design of the deflection coils for correcting the distortion electron-optically.

ALTERNATIVE DEFLECTION SYSTEMS

Although difference current drive gives satisfactory results, it adds to the complexity of the deflection circuits and to the number of adjustments they require. From a receiver manufacturer's point of view, this is scarcely a recommendation. A deflection system that did not necessitate difference current drive would certainly be preferable. However, such a system would have to be based on a deflection yoke design which, being closer to the limit of what is practicable, would call for closer manufacturing tolerances.

Essentially, there are only two practical deflection system configurations suitable for use with a conventional, large screen, 110° shadowmask tube:

— a combination of toroidal coils for both horizontal and vertical deflection,
— a combination of saddle-shaped coils for both horizontal and vertical deflection.

(Toroidal for one deflection and saddle-shaped for the other is not practical, as this results in too much separation between the deflection planes.)

Toroidal coils

Fig. 28 illustrates the principle of a toroidal deflection coil. A symmetrical pair of windings is energized so as to generate oppositely directed fields which tend to force each other out of the toroidal core. The lines of force that are encircled by the core constitute the deflection field; those that extend outwards into the surrounding space constitute an unwanted but unavoidable leakage field. (Owing to this leakage field, a toroidal deflection coil is less sensitive than a saddle-shaped one with a core of comparable size.)

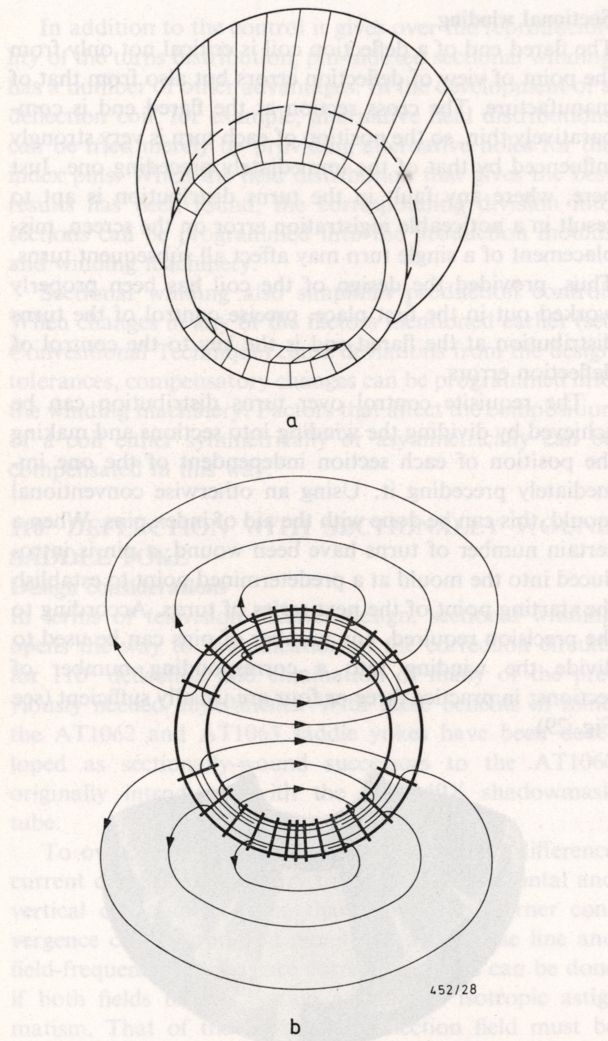

Fig. 28—(a) Flared toroidal core with one pair of windings. (b) Section through a toroidal coil showing the paths of the lines of force

The distribution of the deflection field and the signs and magnitudes of the field parameters ($H_2(z)$, $H_4(z)$, etc.) depend, as in a saddle-shaped coil, on the current density distribution and hence on the turns distribution (Ref. 10). The principal design variables available in existing toroidal coils for influencing the field distribution are:

- the internal contour of the core,
- the current density distribution over the internal surface of the core as a function of angular position.

Owing to the geometry of the construction, there is less freedom to vary the angular current density distribution along the axis of the coil than in a saddle-shaped coil. Thus, it is correspondingly more difficult to modify the form of $H_2(z)$ in different parts of the field. This is a rather important design limitation.

Fig. 28 shows only a single pair of windings on the core, but in practice two are necessary, one for the horizontal deflection and one for the vertical deflection. Moreover, to give the desired field distributions, they will to some extent either have to overlap or be interwound with each other. Mechanical interference between the turns of separate coils, therefore, must be reckoned with in both design and manufacture.

Magnetic interference may also have to be reckoned with. Ideally, the strong magnetic coupling between parts of the horizontal and vertical deflection coils ought to be self-cancelling, but owing to manufacturing tolerances it may not be. In that case, the line flyback pulse will induce an unwanted current in the vertical deflection coil. (Similar coupling also occurs in saddle-shaped coils but can be neutralized by slightly rotating one coil during assembly; with toroidal coils this is not possible.)

Toroidal coils may be wound in one layer or several. If several, then the turns-positioning of any one layer will influence that of the next to an extent depending on wire gauge and pitch. If wound in one layer, then comparatively heavy gauge wire has to be used to carry the large current required. To ensure the requisite accuracy of turns-positioning, notched or grooved locating rings have to be provided at each end of the core. Even so, a coil that is single-layer at the large end of the core may be partly or wholly double-layer at the small end; in between, in the transition region, interference between turns will cause a certain amount of positional inaccuracy.

Tolerances applicable to all of these factors can have an unfavourable effect on the reproducibility of toroidal coils. Moreover, because of the way the deflection field is generated in a toroidal coil, its distribution is more sensitive to dimensional spreads and inhomogeneities in the material of the core than is the case for saddle coils.

Counterbalancing these drawbacks to some extent is the comparative ease with which design changes can be put into effect without serious modification of the tooling. An additional advantage is that a complete set of toroidal coils can be wound on a unitary ferrite core, no subsequent assembly or adjustment being necessary.

Saddle-shaped coils

In a saddle-shaped coil, the ferrite core partly encloses the windings, providing a low-resistance path for closing the magnetic circuit. The leakage field is small, so deflection sensitivity is comparatively high and the current required, low. Furthermore, since the core and the coils are both made up of separable halves, there is some scope for adjusting their relative positions during assembly to optimize performance. On the other hand, a complete deflection assembly with saddle-shaped coils is a more complicated structure than one with toroidal coils.

From the discussion on deflection error theory, it is apparent that, in theory at least, a saddle-shaped coil can be designed to keep deflection errors to an acceptable minimum. The difficulty is, however, that such a coil commonly consists of a large number of turns, the relative positions of which have to be closely controlled. Because of fifth and higher order errors, for deflection angles as large as 110°, turns-positioning is especially critical—too critical in fact to be satisfied by conventional winding techniques. When there was no practical alternative to the conventional techniques, difference current drive was the only way to obtain satisfactory reproduction from a conventional shadowmask tube with a saddle-shaped deflection yoke. Recent refinements in winding technique have now changed the situation, however. Though these refinements are not in themselves complicated, description and explanation of them justifies discussing the manufacture of saddle-shaped coils in some detail.

DEFLECTION COIL MANUFACTURE

Conventional technique

Saddle coils are wound in separable moulds, shaped to the required contours of the windings. The shape of the winding cavity varies from place to place in the mould in accordance with the desired ampere-turn concentration. However, to accommodate the same number of turns throughout, the cross-sectional area perpendicular to the lay of the turns is constant.

The wire is coated with a thermoplastic resin. When the required number of turns has been laid, the winding is heated by a pulse of current and, while still hot, is compacted by means of a plunger to stabilize its shape. It is then separated from the mould.

Winding machines are of two kinds: in one the mould is stationary and wire is fed into it by a rotating 'flyer'; in the other the mould rotates and wire is fed into it from a fixed guide wheel. With either type, 'wings' projecting from parts of the mould may be used to help guide the wire into the cavity.

Within this general scheme, several variations are possible. The mould, for example, may be adjustable to allow some variation in the shape of the winding. For a coil of specified impedance, there is some latitude in the choice of wire gauge and number of turns. Also, two or more wires may be wound at once to be later connected either in series or in parallel.

A number of factors affect the reproducibility of coils manufactured in this way. Foremost is shape; coils with pronounced changes in diameter or thickness are more difficult to duplicate than compact coils with relatively uniform diameter and thickness. The number of turns is also important; the more there are, the less a position error of one turn will affect the properties of the coil. Winding more than one wire at a time also has an effect, particularly when a stationary mould is used; twists introduced by the rotating flyer may cause substantial differences from coil to coil in the positioning of turns. Finally, there are a number of other parameters that may vary during production and so lead to variations in the properties of the coils produced. Among these are: the surface condition of the mould, the wings, and the wire; the temperature of the mould; the diameter and tension of the wire; the winding speed; and the behaviour of the wire feeding and guiding mechanism.

Bringing all these factors under close enough control to keep the tolerances of the product within the very narrow limits required by 110° deflection would be prohibitively expensive. However, there is a much more practical and economical alternative—and one that turns out to be of value in the design and development of deflection coils as well as their manufacture.

Sectional winding

The flared end of a deflection coil is critical not only from the point of view of deflection errors but also from that of manufacture. The cross section at the flared end is comparatively thin, so the position of each turn is very strongly influenced by that of the immediately preceding one. Just here, where any fault in the turns distribution is apt to result in a noticeable registration error on the screen, misplacement of a single turn may affect all subsequent turns. Thus, provided the design of the coil has been properly worked out in the first place, precise control of the turns distribution at the flared end is the key to the control of deflection errors.

The requisite control over turns distribution can be achieved by dividing the winding into sections and making the position of each section independent of the one immediately preceding it. Using an otherwise conventional mould, this can be done with the aid of index pins. When a certain number of turns have been wound, a pin is introduced into the mould at a predetermined point to establish the starting point of the next series of turns. According to the precision required, any number of pins can be used to divide the winding into a corresponding number of sections; in practice three or four are usually sufficient (see Fig. 29).

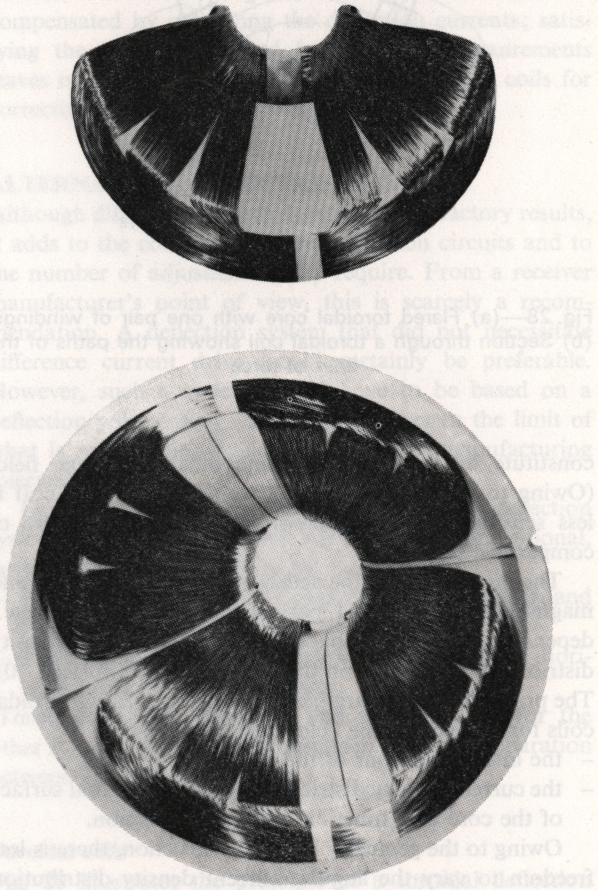

Fig. 29—One winding (top) of a sectionally wound horizontal deflection coil, and the complete coil (bottom) seated in its housing. Note the gaps separating the three sections of each winding at the flared end

In addition to the control it gives over the reproducibility of the turns distribution, pin-indexed sectional winding has a number of other advantages. In the development of a deflection coil, for example, alternative field distributions can be tried merely by providing alternative holes for the index pins. When the field distribution that gives the best results has been found, the corresponding division into sections can be programmed into the production moulds and winding machinery.

Sectional winding also simplifies production control. When changes in any of the factors mentioned earlier (see Conventional Technique) cause deviations from the design tolerances, compensatory changes can be programmed into the winding machinery. Factors that affect the composition of a coil either symmetrically or asymmetrically can be compensated in this way.

110° DEFLECTION WITH SECTIONALLY WOUND SADDLE YOKE

Design considerations

In terms of television receiver design, sectional winding opens the way to simplification of the correction circuits for 110° deflection and elimination of many of the previously needed adjustments. With these benefits in mind the AT1062 and AT1063 saddle yokes have been developed as sectionally-wound successors to the AT1060 originally introduced with the A66-140X shadowmask tube.

To overcome the difficulties associated with difference current drive, it is necessary to design the horizontal and vertical deflection coils so that satisfactory corner convergence can be obtained merely by adding the line and field-frequency convergence corrections. This can be done if both fields have a certain amount of isotropic astigmatism. That of the horizontal deflection field must be relatively small (in order not to impair beam landing), while that of the vertical deflection field must be relatively large (even larger than is usual with 90° deflection). With static convergence, the spot triads will then be as shown in Fig. 30. The line-frequency dynamic convergence corrections needed for red and green are somewhat smaller than with the AT1060 yoke, and those for blue, somewhat larger. The field-frequency corrections for red and green are distinctly larger than with the AT1060, while those for blue are zero, or even slightly negative.

Fifth-order errors, which play a much larger part at 110° than at 90°, tend to make beam landing critical when the astigmatism of the two fields is chosen so that good corner convergence is obtainable by adding the line and field-frequency corrections. The way out of this difficulty is to use a combination of coils which, while keeping the isotropic astigmatism within acceptable limits, gives a certain amount of over-convergence in the corners. Provided the over-convergence is about equal for all three beams, it can be quite easily compensated by equally modulating the line-frequency convergence currents with a field-frequency parabola. The required modulation depth is 25%.

With deflection coils designed along these lines there is a convergence error in the form of a red-green crossover in the middle of each quadrant of the screen. (This is due, in part, to the convergence corrections along each axis being proportional to even powers of one or the other deflection, whilst the errors due to anisotropic astigmatism are proportional to products of the two deflections). However, it is easy to correct this by driving the two halves of the vertical deflection coil asymmetrically at the second harmonic of the line frequency with a current derived from the North-South raster correction circuit.

To minimize curvature of field the AT1062 and AT1063 deflection yokes are 3·5mm longer than their predecessor, the AT1060. The added length increases the deflection sensitivity by about 10% while maintaining adequate margin for axial adjustment; colour purity adjustment by the 'red ball' method is still possible.

Test results

Fig. 31 shows the average residual covergence errors in the corners of a 490mm × 350mm rectangle on the screen, as

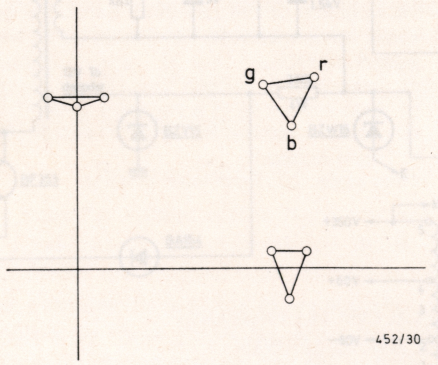

Fig. 30—Spot triad distortions due to horizontal, vertical, and diagonal deflections in a 110° tube using the AT1062 deflection yoke (with static convergence only)

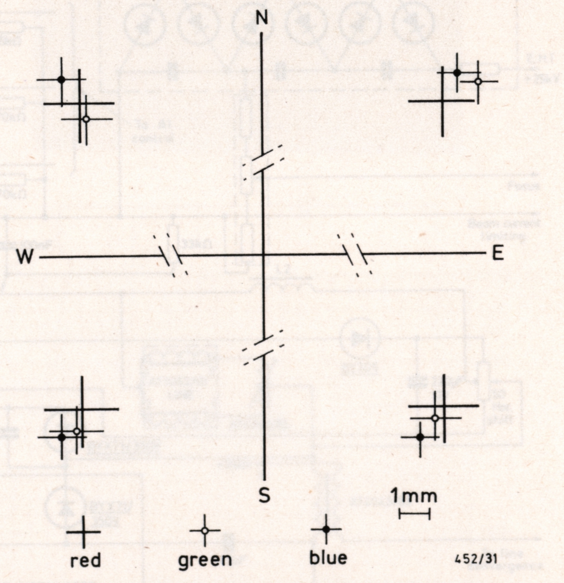

Fig. 31—Residual corner convergence errors of blue and green measured with respect to red. (Average of random samples taken from AT1062 pilot production. Measurements taken at the corners of a 490mm × 350mm rectangle on the screen of an A66–140X picture tube)

measured with random samples of the AT1062 taken from pilot production. For the great majority of samples, the spread with respect to the averages shown was within 0·5mm. For a small percentage of samples, the horizontal or vertical distance between red and green in one of the corners was as large as 1·5mm; for a still smaller percentage the distance was as large as 2mm. With the lateral dynamic correction disabled, the maximum blue lateral error was no more than 1mm in most cases, with a few exceptions as large as 1·5mm. Red-green crossover in the quadrant centres did not exceed 0·5mm in most cases; in a few extreme cases crossovers as large as 1mm were measured.

By narrowing the spread in deflection system characteristics, the sectionally-wound AT1062 and AT1063 saddle yoke assemblies make it possible to adopt a new approach to the design of deflection circuitry for the A66-140X and A56-140X shadowmask tubes. Except for a few additional elements requiring no adjustment, the circuits are of comparable simplicity to those for 90° deflection, and with respect to convergence and beam landing the resulting picture quality is also comparable. Moreover, these improvements are achieved at no cost to the deflection sensitivity.

REFERENCES

1. Glaser, W., **Zeitschrift für Physik**, Vol. 111, 1938, pages 357 to 372.
2. Wendt, G., **Telefunkenröhre**, Vol. 15, 1939, pages 100 to 136.
3. Hutter, R. G. E., **Journal of Applied Physics**, Vol. 18, 1947, pages 740 to 758; 797 to 810.
4. Haantjes, J. and Lubben, G. J., **Philips Research Reports**, Vol. 12, 1957, pages 46 to 48.
5. Haantjes, J. and Lubben, G. J., **Philips Research Reports**, Vol. 14, 1959, pages 65 to 97.
6. Kaashoek, J., **Philips Research Reports Suppl.**, Vol. 11, 1968.
7. Vonk, R., **Philips Technical Review**, Vol. 32, 1971, pages 61 to 72.
8. Kaashoek, J., **Philips Technical Review**, Vol. 32, 1971, pages 34 to 38.
9. Kaashoek, J., **Philips Technical Review**, Vol. 32, 1971, pages 90 to 106.
10. Kaashoek, J., **Philips Technical Review**, Vol. 32, 1971, page 67.

Phase II horizontal deflection circuit and its design principles

UDC 621.397.334

This two-part article describes the horizontal deflection circuit for the Phase II 110° colour receiver, and outlines the safety precautions on which the design is based.

INTRODUCTION

A horizontal deflection circuit, Fig. 1, has been developed specifically for the new 110° deflection coil AT1062 and the colour picture tube A66-140X.

The horizontal output transistor drives the deflection coil direct, therefore the output transformer need handle only the power for the 25V supply and for the e.h.t., and about 7% of the deflection current for E-W correction.

The voltage required by the deflection circuit is about 145V. With the 25V generated by the modulator circuit and the 15V drop across the protection resistor, a supply of 185V is needed.

HORIZONTAL OUTPUT STAGE

The output transistor is a BU208 which drives the AT1062 deflection coil direct via a 470nF capacitor for S-correction. The inductance of the coil connected in parallel is about 1·2mH. The transients which might otherwise be caused by stray inductance in the horizontal output transformer are thus avoided. The lower end of the deflection coil is connected to the E-W diode modulator.

The d.c. collector current of the BU208 is supplied via the primary of the horizontal output transformer, the AT2063. The e.h.t. overwind is connected to a silicon voltage trebler LP1194/40, and is tuned to the fifth harmonic. Because of the distributed capacitance of the primary and the e.h.t. overwind, the flyback pulses at the collector of the BU208 and across the auxiliary windings are virtually sinusoidal. The voltage waveform at the e.h.t. coil shows a slight dip. The low internal resistance of the e.h.t. is due to the wide conduction angle.

A clamping circuit in the trebler cuts off the ringing voltage of the e.h.t., thus stabilising the picture width at beam currents below 0·3mA. The screen grids of the picture tube get their supply (about 1000V) via the load resistance of the clamping circuit. As can be seen from Fig. 2, this voltage is scarcely affected by beam current. As mentioned earlier, the power actually handled by the output transformer is that required by the e.h.t. and the 25V supply. As far as the deflection current itself is concerned the transformer acts mainly as a choke; only the current that modulates the deflection current flows through the secondary (8–9), therefore a small transformer core can be used.

This article is based on work performed in the application laboratories of Mullard and Philips (Eindhoven).

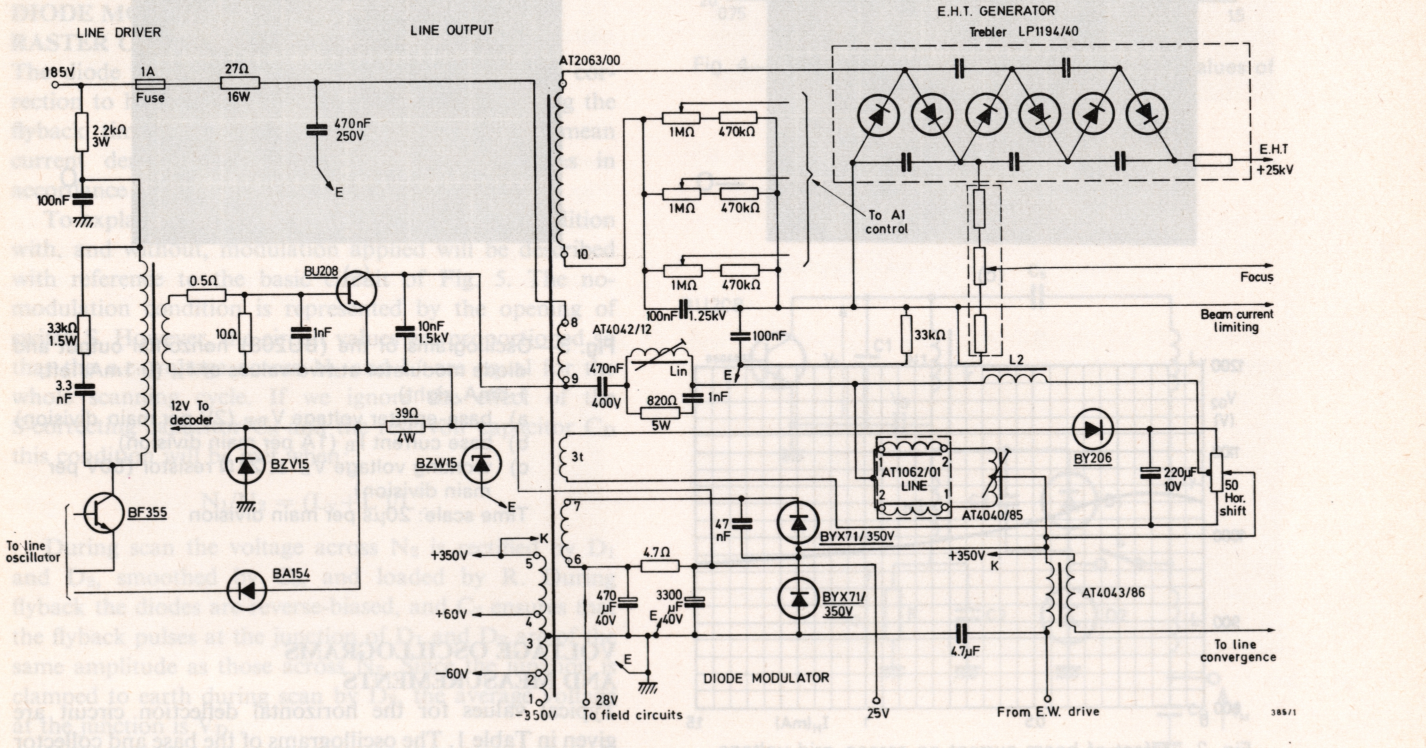
LINE DRIVER
LINE OUTPUT
185V
1A
Fuse
27Ω
16W
2.2kΩ
3W
470nF
250V
E
100nF
AT2063/00
10
BU208
0.5Ω
10Ω
1nF
10nF
1.5kV
3.3kΩ
1.5W
3.3 nF
12V To decoder
39Ω
4W
BZV15
BZW15
BF355
To line oscillator
BA154
+350V
K
+60V
−60V
−350V
28V
To field circuits
1
2
3
4
5
6
7
8
9
3t
AT4042/12
470nF
400V
Lin
820Ω
5W
1nF
1MΩ
470kΩ
100nF
1.25kV
To A1 control
E.H.T. GENERATOR
Trebler LP1194/40
E.H.T
+25kV
Focus
Beam current limiting
33kΩ
L2
BY206
220μF
10V
50
Hor. shift
AT1062/01
LINE
AT4040/85
47 nF
BYX71/350V
4.7Ω
470 μF 40V
3300 μF 40V
AT4043/86
4.7μF
To line convergence
DIODE MODULATOR
25V
From E.W. drive
385/1

Figure 1. Horizontal deflection circuit

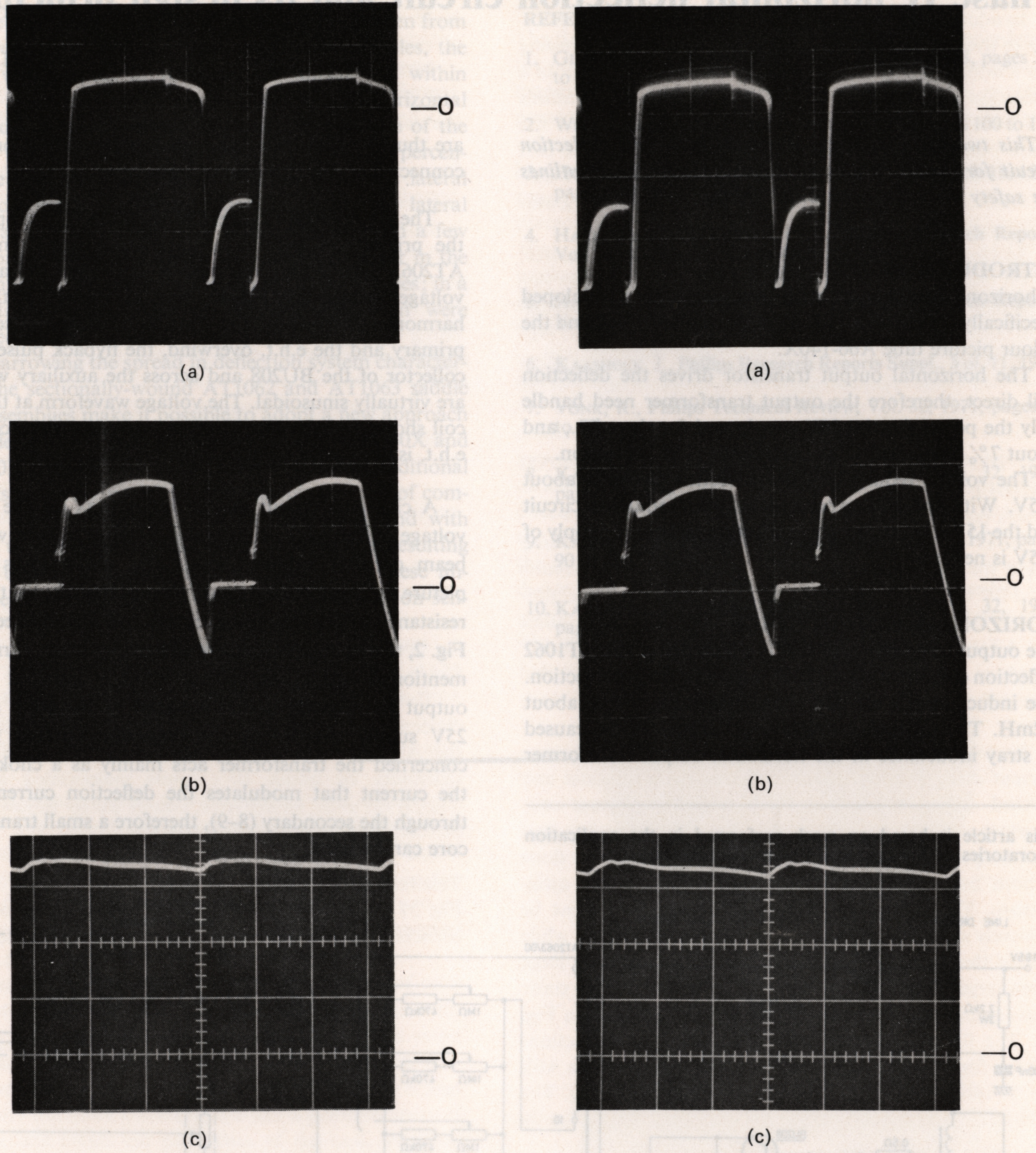

Fig. 3—Oscillograms of the (BU208) horizontal output and diode modulator at two values of I_H (0·1mA, left; 1·5mA, right)

a) base-emitter voltage V_{BE} (2V per main division)

b) base current I_B (1A per main division)

c) working voltage V_B' at 27Ω resistor (50V per main division)

Time scale: 20µs per main division

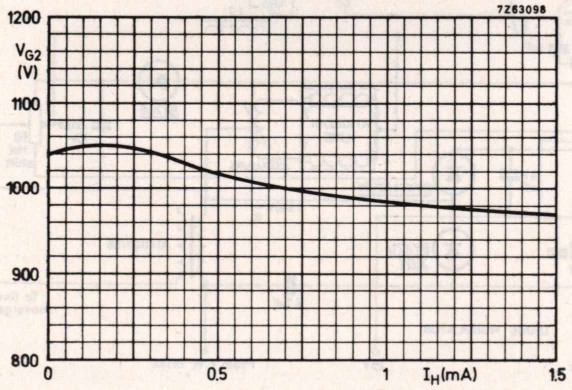

Fig. 2—Effect of beam current on screen-grid voltage (A66-140X picture tube with AT1062 deflection assembly)

VOLTAGE OSCILLOGRAMS AND MEASUREMENTS

Typical values for the horizontal deflection circuit are given in Table 1. The oscillograms of the base and collector circuits of the BU208 are given in Fig. 3. With an e.h.t. of 25kV the deflection coil requires a current of about 6A. If the voltage across the S-correction capacitor and the linearity control are taken into account a total deflection voltage of 145V is needed. Bearing in mind that the emitter of the BU208 is connected to the 25V supply and that there is a voltage drop across the 27Ω series resistor, a supply (V_B) of 185V is needed. This voltage must be stabilised against mains voltage fluctuations.

The horizontal output stage was loaded with passive blue lateral convergence and passive horizontal convergence circuits. The 25V line supplies the vertical deflection circuit, the E-W drive circuit, and a resistor that represents the loads normally taken by the other circuits. Current drain is 1·5A.

TABLE 1

Typical values with BU208 and diode modulator

Beam current (I_{beam})	0	1·1	1·5	mA
Supply voltage	185	185	184	V
Voltage at pin 8	172	168	166	V
I_{av} (supply line)	480	610	658	mA
V_{eht}	25	22·4	21·9	kV
V_{CEM}	1200	1160	1140	V
I_{CM}	3·9	3·95	4·0	A
I_{defl}(pk-pk)	6·00	5·80	5·75	A
Flyback time	11·7	11·8	11·9	µs
Internal impedance ($\Delta V_{eht}/\Delta I_{beam}$)		2·1		MΩ
V_{28}	29·0	28·2	28·2	V
V_{25}	25·0	24·8	24·8	V
Variation in overscan		1·5		%

LOW VOLTAGE SUPPLY

The d.c. voltage of about 28V at point 8 of the horizontal output transformer should be loaded to a minimum of 0·75A. It can be used for the low-voltage supply. The recovery diode, a BYX71, and the forward diode, a BYX71, which has also to supply the current for the output stage of the E-W correction circuit, are rated at 1·5A. The 25V supply can then deliver 1·5A (37W), which is sufficient for the vertical output stage, vertical dynamic correction circuit, the E-W drive, the decoder, tuner and i.f. stages, and audio. Fig. 4 shows that the 25V supply is virtually independent of e.h.t. loads. With higher e.h.t. loads the voltage at point 6 drops, but the current through the BU208 output transistor increases. With a suitably chosen series resistor (4·7Ω) the effects cancel.

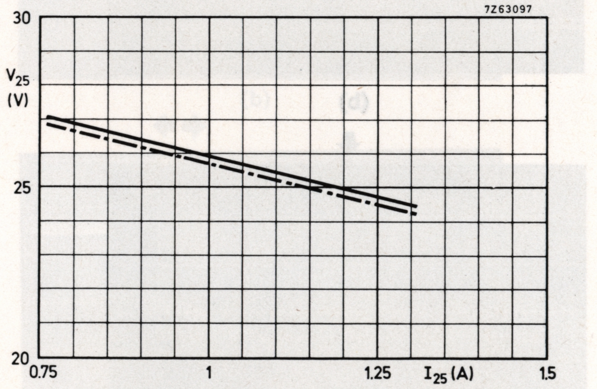

Fig. 4—Effect of load I_{25} on 25V supply for two values of beam current, I_H = 0mA (————) and I_H = 1·5mA (— — —)

DIODE MODULATOR FOR E-W RASTER CORRECTION

The diode modulator circuit provides the required correction to horizontal scan current whilst maintaining the flyback time and e.h.t. potential constant. The mean current demanded from the power supply varies in accordance with the modulation.

To explain the operation of the system, the condition with, and without, modulation applied will be described with reference to the basic circuit of Fig. 5. The no-modulation condition is represented by the opening of switch S. However, the circuit values are proportioned so that the a.c. voltage across N_2 and L' are equal for the whole scanning cycle. If we ignore the effect of the S-correcting capacitor C_S and the reservoir capacitor C_D this condition will be met when:

$$N_1/N_2 = (L_y+L')/L'.$$

During scan the voltage across N_2 is rectified by D_1 and D_2, smoothed by C_3, and loaded by R. During flyback the diodes are reverse-biased, and C_2 ensures that the flyback pulses at the junction of D_1 and D_2 are of the same amplitude as those across N_2. Since the junction is clamped to earth during scan by D_2, the average voltage at the junction is V_D.

If the switch is now closed, and no external drive is applied to C_D, the voltage across C_D will be equal to V_D.

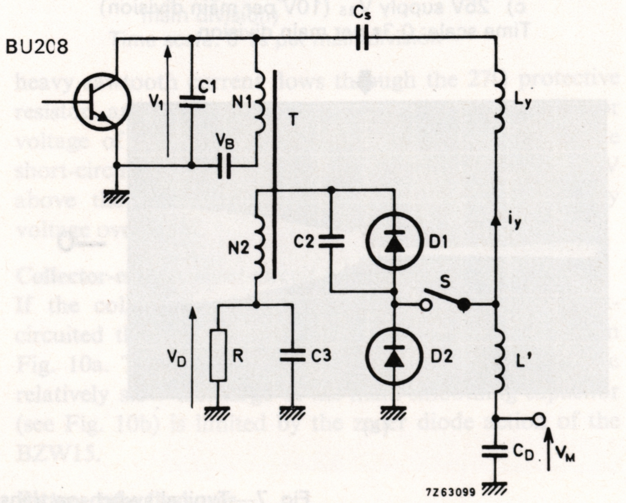

Fig. 5—Basic diode modulator

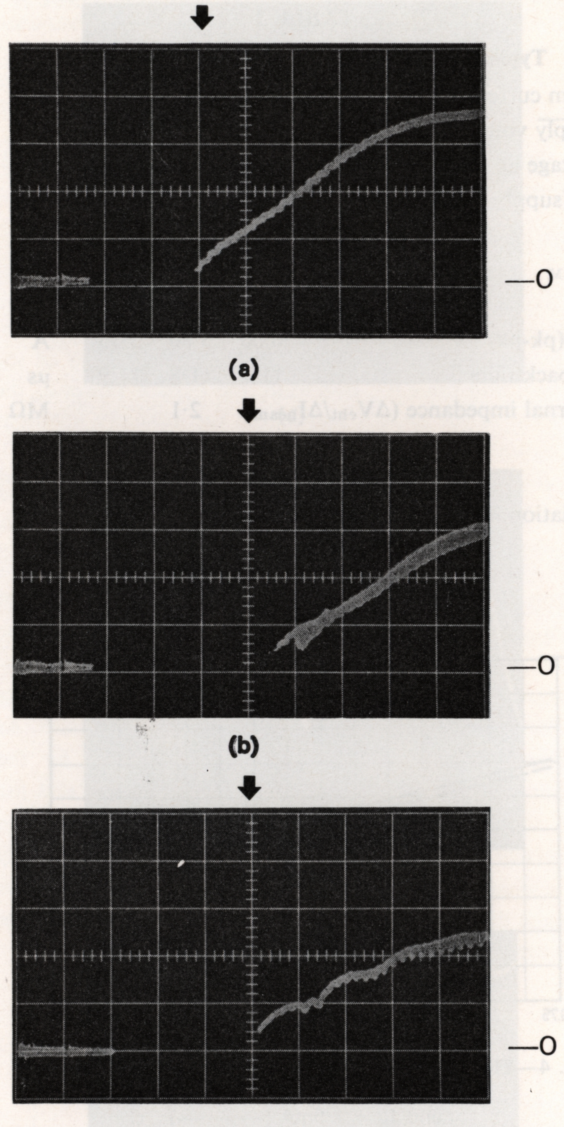

(a)

(b)

(c)

Fig. 6—Typical switch-on transients
a) working voltage V_B' (50V per main division)
b) working voltage V_B' at 27Ω resistor (50V per main division)
c) 25V supply V_{25} (10V per main division)
Time scale: 0·3s per main division

The flyback time in this condition is proportional to:

$$\sqrt{[(L_y+L')C_1]}.$$

A further condition must now be imposed to ensure that the tuning of transformer T is unaffected when the modulator is driven by varying the voltage across C_D. Assume now that C_D is bridged ($V_M = 0$). The average voltage at the junction of the diodes must now be zero (ohmic connection to earth via L′). Furthermore, since diode D_2 conducts the 'on-state' currents to earth, there can be no significant a.c. voltage at this point.

The coil L_y is now in parallel with N_1, and capacitor C_2 is in parallel with N_2. Thus the flyback time is proportional to

$$\sqrt{[C_1+(N_2/N_1)^2C_2]L_y}$$

and for equal flyback time,

$$C_1\,(L_y+L') = L_y\,[C_1+(N_2/N_1)^2\,C_2].$$

Since the operating voltage V_B is also constant (because of power supply filtering) the deflection current is increased by a factor

$$(L_y/I_0 = 1+(L'/L_y).$$

The deflection current may be set by values of V_M between V_D and zero to whatever level is required for correct picture width or E-W raster correction, whilst the flyback voltage at the BU208, and hence the input voltage to the trebler, are constant and unmodulated.

When the modulator voltage V_M is at zero, an important requirement exists for the load resistor R. Since during the first half of scan the deflection path is:

$$BU208\rightarrow C_S\rightarrow L_y\rightarrow D_1\rightarrow N_2\rightarrow C_3$$

and for the second half

$$D_2\rightarrow L_y\rightarrow C_S\rightarrow BU208.$$

the current bleed via R must be sufficient to ensure that the charge on C_3 does not build up to a level at which V_D exceeds $V_B(N_2/N_1)$. If this build-up occurs, the deflection current will be reduced and the modulator will be ineffective.

TRANSIENTS AND PROTECTION

Switch-on behaviour

Figs. 6 and 7 show what happens to the supply voltage and to the voltage and current of the collector when the power supply is switched on. The power supply features a slow-start circuit which ensures that the final output voltage is reached after about 1·5s. The rise is gradual and there are no indications of overshoot. This is also true of the collector current and voltage of the BU208, and of the 25V supply.

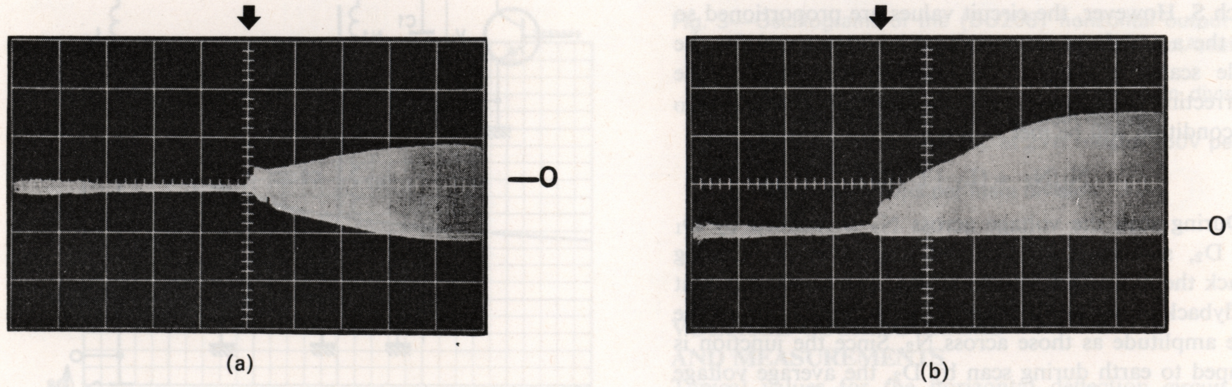

(a) (b)

Fig. 7—Typical switch-on transients — Time scale: 0·3s per main division
a) collector current (BU208) I_C (4A per main division)
b) collector voltage V_{CE} (500V per main division)

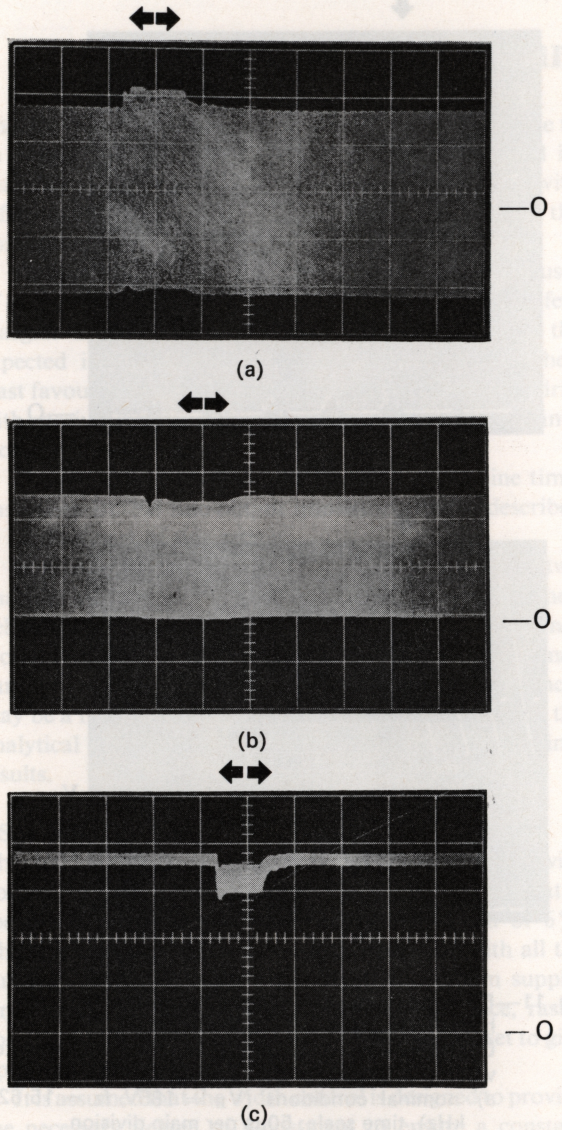

(a)

(b)

(c)

Fig. 8—Short circuit of the 25V supply
a) collector current (BU208) I_C (2A per main division)
b) collector voltage V_{CE} (500V per main division)
c) working voltage V_B' at 27Ω resistor (50V per main division)
Time scale: 0·1s per main division

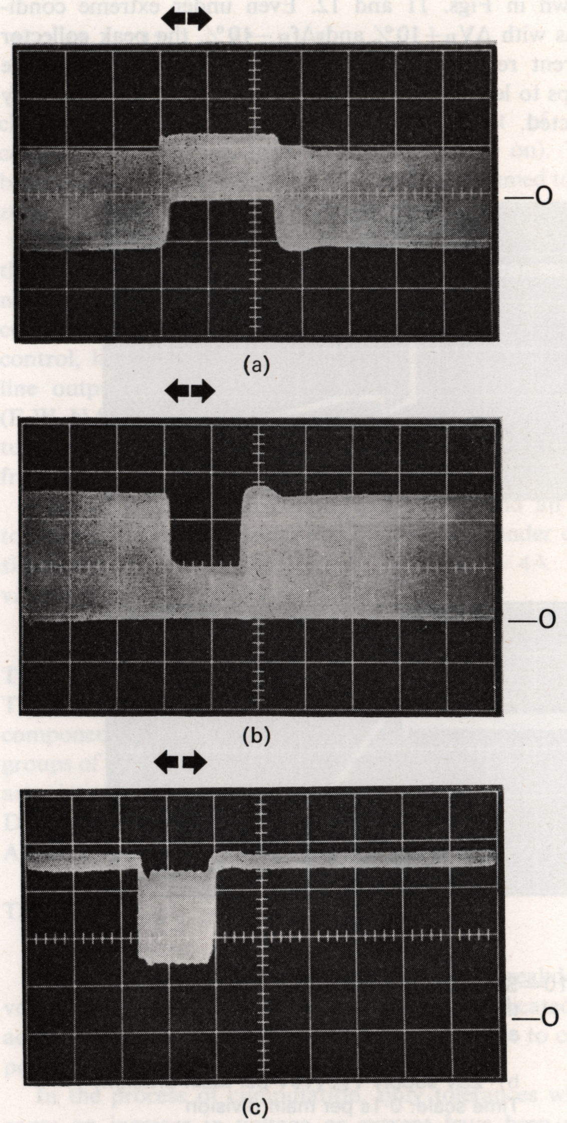

(a)

(b)

(c)

Fig. 9—Short circuit at pin 8 of AT2063 transformer
a, collector current (BU208) I_C (4A per main division)
b, collector voltage V_{CE} (500V per main division)
c, working voltage V_B' at 27Ω resistor (50V per main division)
Time scale: 0·1s per main division

Short-circuit of 25V supply

Fig. 8 shows the effect of short-circuiting the 25V supply. There is an increase of I_{CM} to 4·5A, while the collector voltage drops because of the increased voltage drop across the 27Ω resistor. (See the lower oscillogram of Fig. 8). In consequence the voltage ratings of the BU208 are not exceeded when the 25V supply is short-circuited.

Short-circuit of the 28V supply

The oscillogram of Fig. 9 was made during a brief short-circuit of the 28V supply at pin 8 of the AT2063. A heavy sawtooth current flows through the 27Ω protective resistor and the transformer, and the peak collector voltage of the BU208 drops to about 500V. When the short-circuit is removed the collector voltage rises to 100V above the operating value, mainly because of supply voltage overshoot.

Collector-emitter short-circuit on BU208

If the collector and emitter of the BU208 are short-circuited the fast-acting h.t. fuse will blow, as shown in Fig. 10a. The increase in the 25V supply caused by the relatively slow discharge of the main smoothing capacitor (see Fig. 10b) is limited by the zener diode action of the BZW15.

Picture tube flashover

Picture tube flashovers were simulated, and the results are shown in Figs. 11 and 12. Even under extreme conditions with $\Delta V_B+10\%$ and $\Delta f_H-10\%$, the peak collector current remains below 7A. The peak collector voltage drops to less than 1kV. The low-voltage supply is scarcely affected.

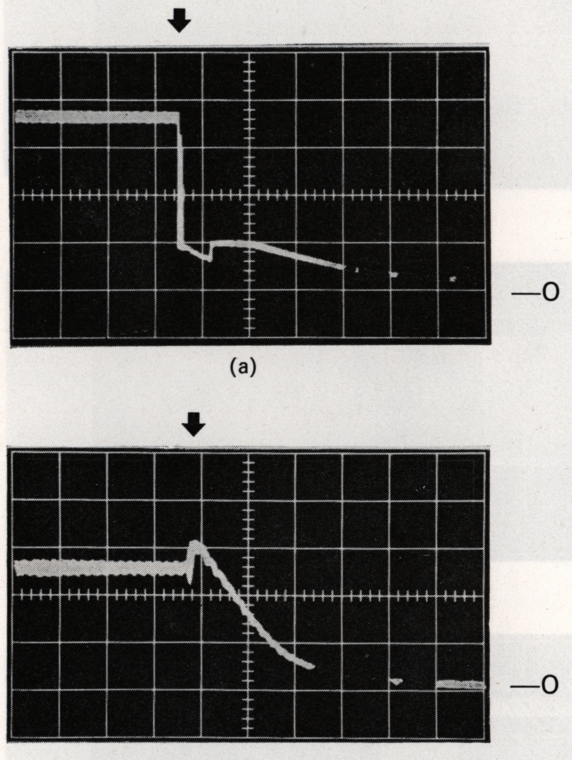

(a)

(b)

Fig. 10—Short circuit between collector and emitter of the BU208
a) working voltage V_B' at 27Ω resistor (50V per main division)
b) 25V supply V_{25} (10V per main division)
Time scale: 0·1s per main division

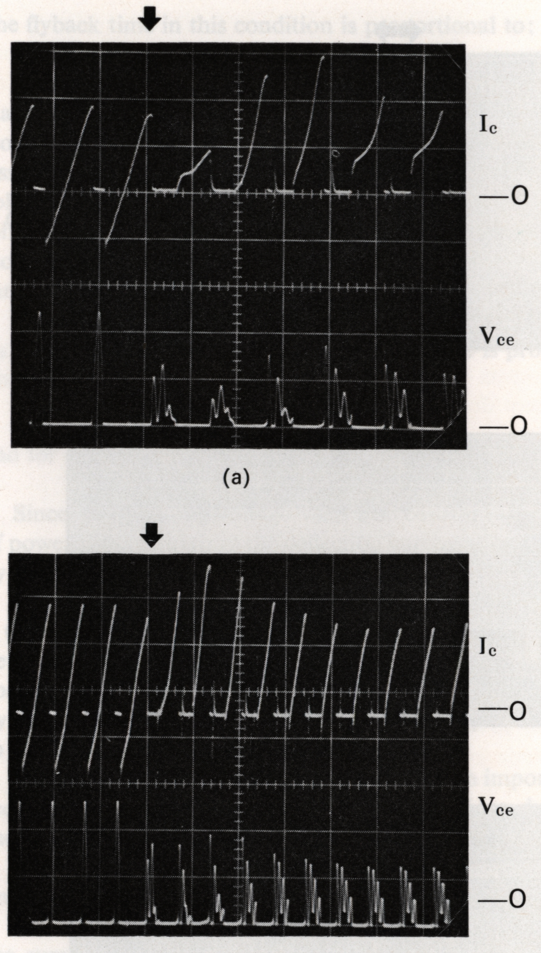

(a)

(b)

Fig. 11—Effect of picture tube flashover on the (BU208) horizontal output and diode modulator
Collector current I_C at 2A per main division, collector voltage V_{CE} at 500V per main division
a) nominal conditions (V_B = 185V, fz = 15·625 kHz), time scale: 50μs per main division
b) extreme conditions (f_z = 14·1kHz), time scale: 100μs per main division

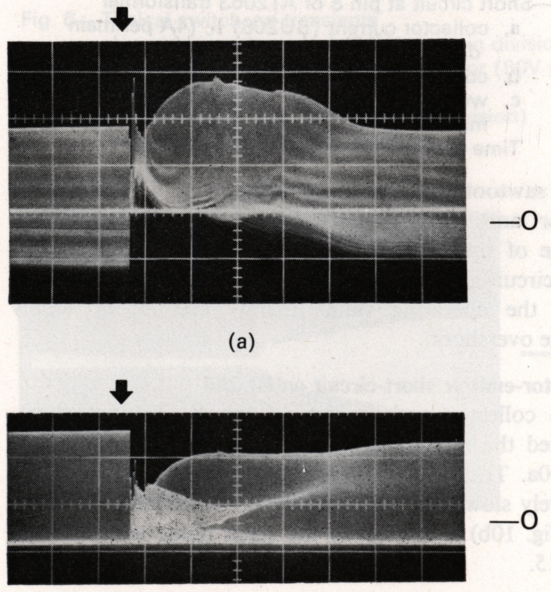

(a)

(b)

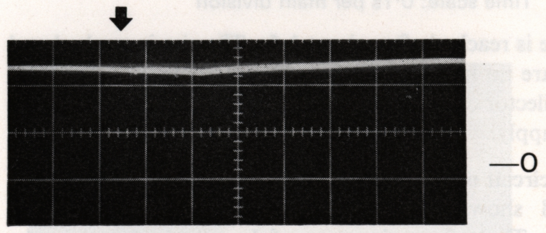

(c)

Fig. 12—Effect of picture tube flashover on the (BU208) horizontal output and diode modulator under nominal conditions
a) collector current I_C (2A per main division)
b) collector voltage V_C (measured with respect to chassis, 500V per main division)
c) 25V supply V_{25} (10V per main division)
Time scale: 1ms per main division

Spreads and tolerances in the line timebase

The line output transistor in a television receiver is liable to be exposed to voltages and currents that may exceed its peak ratings. Therefore the receiver must be designed with safety margins that will obviate such occurrences and the possible consequent damage to the transistor.

This section comprises an analysis of the possible causes of excessive voltages and currents, and evaluates the safety margins that must be built in. The calculations cover the expected initial spreads of component values and their least favourable combinations, operational variations, drift with receiver life, and adjustments during receiver manufacturing and servicing.

The analysis is based on the Phase II colour line timebase, with BU208 line output transistors, that is described in the first part of this article.

It must be admitted, at the outset, that there are no two analyses exactly alike. Component tolerances and their behaviour with life may differ from one component manufacturer to another. Acceptable operational variations may vary from setmaker to setmaker. The effect of tolerances may be a function of individual circuit variations. Even the analytical approach taken may have a bearing on the final results.

ASSUMPTIONS

The 100% VA level refers to a line timebase fitted with nominal components and scanning a nominal tube at a specified e.h.t. and with the prescribed overscan of 6%. The timebase is synchronised and is operating with all the auxiliary loads connected to it (scan rectification supply, c.r.t. heater, A_1 supply, and so on). Convergence, raster correction, linearity control, and S-correction are set to give optimum performance.

It is assumed that the width control is designed to provide the necessary degree of adjustment to ensure a constant raster width in the presence of normal spreads (but excluding out-of-sync operation, misadjustment of h.t. control, abnormal h.t. load variations, and so on). The beam current drawn from the e.h.t. supply is assumed to be zero.

Therefore, in evaluation of the corresponding VA of the timebase under nominal operating conditions, it is necessary to take into account both the VA of the deflection coils and the additional loads due to: 6% overscan, width control, linearity control, S-correction, inductance of the line output transformer, convergence, raster correction (E-W, N-S), scan rectification and other supplies, transistor turn-off time, and (most important) the beam current drawn from the e.h.t. supply.

The value so obtained represents 100%, and all the tolerances are referred to it. For the timebase under consideration this level corresponds to i_c(pk) = 4A and v_c (pk) = 1·2kV.

TOLERANCES

The tolerances are listed in four tables. Table 2 deals with component spreads; are these added statistically. The other groups of tolerances, each of which is added arithmetically, are given in: Table 3, Operational Tolerances, Table 4, Drift with Life, and Table 5, Manufacturing and Servicing Adjustments.

All tolerances are summarised and added together in Table 6.

Since a transistor is destroyed when its collector breakdown voltage is exceeded, it is necessary, as already indicated, to add the tolerances arithmetically, except those due to component spreads.

In the process of computation, only tolerances which cause an increase in voltage or current have been considered. Whilst there is some logic in this approach, the

TABLE 2

Components spreads

	Unit	**Tolerance** (%)	**Effect of the tolerance** Δi_c (%)	Δv_c (%)	Δ_{scan} (%)
Deflection coil inductance, L_y	mH	3·0	2·7	1·7	2·4
Deflection coils sensitivity, $L_y i_y$	—	2·0	1·8	1·3	1·6
Picture tube sensitivity	—	1·5% scan	—	—	1·5
Effects of width control adjustment	—	—	1·0	1·0	—
Line output transistor inductance 10L_y	mH	10	0·3	0·2	0·3
Line output transistor defl. coil turns ratio	—	0·5	0·5	0·3	0·5
Accuracy of harmonic tuning	%	10	0·5	0·5	0·3
Line output transistor+defl. coil capacitance	pF	5·0	—	1·25	1·1
Tuning capacitor	pF	5·0	—	1·25	1·1
S-correction capacitor	pF	10	2·0	0·5	2·0
Line output transistor turn-off time	—	—	—	1·0	0·5
Flashover protection resistance	Ω	required	—	1·0	1·0
Passive convergence		range	1·0	0·5	2·0
H.T. voltage setting	V	1·0	3·0	3·0	2·7
L.T. supply load variations	A	20	1·0	1·0	0·9
R.M.S. sum:			5·2	4·6	5·7

TABLE 3

Operational tolerances

	Unit	Tolerance	Effect of tolerance		
		(%)	Δic(%)	Δvc(%)	Δscan(%)
Mains voltage	V	±10	±2·0	±2	1·0
Beam current 0 to 1·5	mA		±9·0*	−5	1·5
Out-of-sync	kHz	−10	+10	+10	—
Arithmetic sum of +ve tolerances:			12	12	2·5

*This tolerance is normally taken into account at the design stage of the line timebase, and is therefore not added

TABLE 4

Drift with life

	Unit	Tolerance	Effect of tolerance		
Tuning capacitor	pF	−5	—	+1·25	−1·1
Line output transistor	pF	−5	—	+1·25	−1·1
S-correction capacitor	pF	−5	−1·0	+0·2	+1·0
Flashover protection resistance	Ω	+5	−0·25	−0·25	−0·35
H.T. line drift	V	±3	3·0	±3·0	±2·7
Arithmetic sum of +ve tolerances:			3·0	5·7	3·7

TABLE 5

Manufacturing and servicing adjustments

	Unit	Total tolerance	Tolerance already accounted for	Net tolerance	Effect of tolerances	
			(%)	(%)	Δi_c (%)	Δv_c (%)
Adjustment of h.t.	V	10	3+3	4	4	4
Adjustment of line frequency	kHz	12	10	2	2	2
Low tension load variation	A	−50	20	−30	+1·5	+1·5
Arithmetic sum of tolerances:					7·5	7·5

TABLE 6

Addition of tolerances

Tolerances	Δi_c (%)	Δv_c (%)	Δ_{scan} (%)
Components	5·2	4·6	5·7
Operational	12·0	12·0	2·5
Drift with life	3·0	5·7	3·7
Manufacturing and servicing	7·5	7·5	—
Arithmetic sum:	27·7	29·8	11·9

likelihood of simultaneous occurrence of all the positive tolerances in one receiver is very small indeed. For instance, in a new receiver there will not be any component ageing. This automatically removes 3% of the total value for current tolerances and 5·7% of the voltage tolerances.

In every case, the maximum tolerance of every parameter is considered. In practice, most of the tolerance will have considerable variations within the assumed absolute error boundary. Therefore there is a reasonable degree of certainty that the summation in Table 6 is too much on the conservative side. Unfortunately, there is no golden rule which would lead to a precise solution of the problem. A reasonable compromise is to ensure that every new receiver is safe under all adverse combinations of tolerances. The margins of safety arising from this approach can be considered as ample allowance for drift of components during life. (In a way, the end of life of a receiver is reached when the total combination of drifts begins to seriously affect its performance.) On this basis, and with some upward rounding-off, the results in Table 6 lead to the following recommendations:

Tolerances in peak collector current
27·7—3·0 = 24·7% (say 25%)

Tolerances in peak collector voltage
29·8—5·7 = 24·1% (say 25%)

OTHER TOLERANCES AND MARGINS OF SAFETY

In the computation of component tolerances it has been assumed that all the spreads considered are independent of each other and, therefore, may be added statistically. This is possible if the spreads are normal (gaussian). Often this approach is criticised on the grounds that the spreads may depart substantially from the ideal, and that the nominal value of a large batch of components may be biased toward one end of the distribution. Examination of Table 2 indicates that the contributions of individual components are small. Even a serious disturbance to the shape of the spread in one or two of them will have only a small effect on the overall tolerance.

So far, no mention has been made of the spreads of line output transistors. Normally, these spreads do not have a square distribution starting at the published value of, say, the collector breakdown voltage.

The margins of safety arising from the interplay of receiver and transistor tolerances are substantial. They have been reserved as a buffer against any discrepancies between calculated values and the realities of television receivers coming off the production line.

CONSEQUENCES

The analysis suggests that the limit values of peak collector current and peak collector voltage can be estimated by adding 25% to the nominal values. Conversely, if the limit values are known, the nominal values can be set at 80% of the limit values.

This conclusion applies also to the peak voltages of many devices connected to the line timebase: e.h.t. rectifiers, A_1 diodes, scan rectification diodes, and so on (and the associated capacitors and other components). But the relationship is somewhat different for other voltages: for instance, scan rectification output voltage, and c.r.t. heater voltage when derived from the line output transformer.

Inevitably, the same argument applies to the e.h.t. supplied to the picture tube. With the nominal operating potential of 25kV, the limit value of 27·5kV is only 10% away, yet the analysis suggests a possibility of 25%: up to 31·3kV. Table 6 shows that the available 10% margin can just about accommodate the spreads of components (4·6%) and, say, drift with life (5·7%). For the rest, it may be helpful to refer to the newly coined phrase: 'the picture tube is a forgiving device'. Occasional overvoltage may cause additional flashover, but the tube will not be destroyed or its life affected.

ANOTHER LOOK AT THE TOLERANCES

To get a clearer impression of the relationship between the various groups of tolerances listed in Table 6, the results are shown graphically in Fig. 13.

One of the largest blocks is taken by operational tolerances (12% out of a total of 29·8%). Out of this, 10% is occupied by the out-of-sync condition (Table 3). Considering that television transmitters are operated asynchronously nowadays, with a high degree of line frequency stability, the range of expected frequency deviation of the line oscillator seems to be very large indeed.

Another block with large tolerance occupancy belongs to the manufacturing and servicing adjustments (7·5%: one quarter of the total). In this case, availability of controls for h.t. and line frequency setting is the cause of such large excursions. Preset potentiometers normally used for these functions are inherently unstable components and, as such, they are also responsible for drifts with life. It seems a pity to take less than full advantage of the capability of a well stabilised power supply by using a component that can produce drifts and which permits an operator to vary the h.t. line indiscriminately. Serious thought should be given to replacing potentiometers in critical applications by fixed resistors.

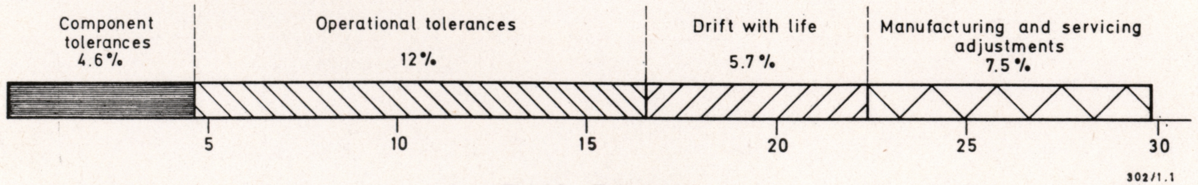

Fig. 13—Tolerances

CONCLUSIONS

A satisfactory provision for spreads of components, operational variations, drifts with life, and manufacturing and servicing adjustments can be made by allowing 25% above the nominal values of peak collector current and peak collector voltage of the BU208 operated in the Phase II colour receiver. This recommendation is based on currently available components and observance of a 'good practice' approach in the design of the receiver.

From the analysis it is quite clear that spreads of components constitute only a small part of the total allowance. The largest single contribution is due to the possible excursion of the line frequency oscillator. This is closely followed by the range of h.t. voltage controlled by the potentiometer in the stabilised h.t. supply. Attention to the design of these items can contribute considerably to the reliability of the receiver, and perhaps eventually to the reduction of cost of the line output transistor.